Fall 2018

Development of a UAV-Based System to Monitor Air Quality over an Oil Field

Siwen Liu
Montana Tech

Development of a UAV-Based System
to Monitor Air Quality over an Oil Field

by

Siwen Liu

A thesis submitted in partial fulfillment of the

requirements for the degree of

Environmental Engineering

Montana Technological University

2018

Abstract

The growth of hydraulic fracturing has pushed the whole petroleum industries forward. As a result, gas (mainly methane [CH_4]) emissions have significantly increased over the past decades (Macey et al., 2014). Gas leaks can occur at almost all stages of a petroleum production process, such as drilling, fracking, and refining. For years, ground-based air quality monitoring has been conducted around production sites. An improved understanding of air quality would be enabled by supplementing ground-based with airborne monitoring. The latter would involve the use of unmanned aerial vehicles (UAVs) to carry a compact, portable air monitoring system. The purpose of this study was to design and fabricate a UAV-based system for monitoring of CH_4 and CO_2, the two most important greenhouse gases, over oil fields. The system consisted of an airborne sensor node and a ground station. The sensor node was comprised of low-cost gas sensors, a microcontroller, a LoRa wireless transmitter, a GPS module, and an SD card shield. The ground station was comprised of a LoRa wireless receiver, a microcontroller, and a laptop. Both the sensor node and the ground station were programmed using Arduino IDE. A graphic user interface (GUI) was created using LabVIEW for data logging and visualization on the laptop. Preliminary trials near the university campus showed that the system was capable of measuring CH_4 and CO_2 concentrations in real time, along with temperature, relative humidity, and GPS location; while sending the monitoring data to the ground station (up to ~800 m away) every two seconds without any loss. The system was further tested at two oil production sites in North Dakota. The results revealed a heterogeneous distribution of CH_4 and CO_2 over the sites, demonstrating a potential application of the system for air quality survey and gas leakage detection. The advantage of this UAV-based monitoring system lies in its portability, expandability, lower cost, ease of deployment and operation. The overall cost of the system was below 300 dollars, and it weighed 540 grams, including enclosures. The system performance was limited by the selected gas sensors with relatively poorer sensitivity and slower response than regular gas monitors (which are bulkier and much more expensive). However, with the advancement in sensor technologies, it is expected that the quality of monitoring data from the UAV-based system can be considerably improved in the near future.

Dedication

   I would like to dedicate this thesis to all my loved ones. I would like to thank my family for being on my side and encouraging me throughout my entire graduate study, as well as their financial support. I would like to thank my all friends for stuck around and giving me mental and physical support during my lowest time. I would like to thank all my teachers, not only for giving me all my great skills but also giving me guidance when I'm lost. Finally, I would like to thank my beloved fiancée, Xiaotang Tang, for staying with me through all these times and giving me tremendous physical and moral support over the years. I won't come this far without anyone who loved me and supported me.

Acknowledgments

First, I would like to thank each member in my thesis committee: Xufei Yang, Raja Nagisetty and Xiaobing Zhou. They offered me a lot of help to accomplish my thesis project. Their great advice helped me developed my professional skills. I am very grateful for their open hours which I could ask endless questions. I would like to thank Xufei Yang especially for serving as my committee chair, without his help and guidance I will never be able to have these skills to finish my project.

I would like to thank Rebecca Morris for helping me with printing my 3D model. As part of the project, it's a huge challenge to construct an enclosure that fits the requirements, with her expertise my design is finally completed.

Finally, I would like to thank Justin Balkenbush and Mike Juma of Iron Oil Operating, LLC for kindly providing me with well sites to test my design and helping me throughout my testing period.

Table of Contents

List of Tables

List of Figures

List of Equations

Chapter 1

1. Literature Review

This chapter is a literature review on all the elements and technologies used in this project, which provides background information and helpful explanations. Key concepts include fugitive methane (CH_4) emission from oil and gas production, and air monitoring systems based on off-the-shelf sensors and unmanned aerial vehicles (UAVs).

1.1. Fugitive CH_4 Emission from Oil and Gas production

As concerns grow over the climate impact of increasing greenhouse gas emissions and the actual and associated political costs of imported fuels, the U.S. is looking to exploit natural gas as a domestic energy source. Natural gas is considered a "cleaner" energy source because its combustion produces more energy per unit mass of carbon dioxide (CO_2) released ($J/g\ CO_2$) than coal and oil (177% and 140%, respectively) (U.S. Department of Energy Energy Information Administration, 1999). However, the climate benefit can be reduced when methane, the major component of natural gas leaks to the atmosphere; and the leakage can take place anywhere from the point of extraction downstream to the point of consumption. Methane (CH_4) is a potent greenhouse gas with its global warming potential (GWP) 25 times higher than that of CO_2 over a 100-year time horizon (Intergovernmental Panel on Climate Change, 2007). Although it is difficult to make an accurate assessment of the exact climate impact of natural gas production, a recent study by Alvarez and his colleagues has suggested that if more than 3.2% of natural gas leaks to the atmosphere on its way from the point of extraction to a gas-fired power plant, the gas-fueled electricity production will have a more substantial immediate climate impact than that from a coal-fired plant (Alvarez, Pacala, Winebrake, Chameides, & Hamburg, 2012).

Numerous estimates of methane emissions from the natural gas industry are available. In a milestone paper "Estimate of Methane Emissions from the U.S. Natural Gas Industry," the authors stated that it is essential to classify the emissions into two categories: steady and unsteady. For emissions that are continuous or relatively steady over long periods, a single series of measurements was sufficient to allow annual emissions to be calculated. For discontinuous or unsteady emissions, sampling a single source for a year or more to determine annual emissions was often infeasible; and the emissions were estimated using available information such as volumes of vessels, cross-sectional areas and flow rates of pipes, duration of events, and frequency of events (Kirchgessner, Lott, Cowgill, Harrison, & Shires, 1999). In the same paper, the authors used three methods to measure steady emissions: component measurement method, tracer gas method, and leak statistics method. The component measurement method directly allocates aerial emissions by basic components in a production system such as valves, flanges, seals and other connectors, determines their respective emissions, and then adds them together to estimate the total emission. The tracer gas method features the releasing of a tracer gas (usually sulfur hexafluoride [SF_6]) at a known constant rate near the emission source and measuring the downwind concentrations of the tracer gas and methane simultaneously. The leak statistics method is used to quantify methane emissions from underground main and service pipelines. Emission rates are measured for a large number of leak case examples to accurately determine the average emission rate per leak as a function of pipe material, age, operating pressure, and soil characteristics (Kirchgessner, Lott, Cowgill, Harrison, & Shires, 1999).

Unsteady emission sources require data gathering and a unique set of equations to quantify the average annual emissions. In general, the following information is needed to quantify annual emissions: 1) detailed technical characterizations of the sources and

identification of the important parameters affecting emissions; 2) data from multiple sites that allow the methane emitted per emission event to be calculated from the governing equations; and 3) data on the frequency of releases. The authors gave an example of estimating methane emissions from a vessel blowdown for routine maintenance. In this case, the volume, pressure, and temperature of gas contained in the vessel before blowdown were used to calculate losses from a blowdown event. Additionally, an average frequency of these vessel blowdown events was necessary to determine the annual loss (Kirchgessner, Lott, Cowgill, Harrison, & Shires, 1999).

A ground-based monitoring network taking continuous samples may be unable to capture a full range of air impacts of unconventional oil and gas (UOG) operations, and oftentimes air concentrations of potentially toxic compounds and chemical mixtures are highly variable near oil and gas production sites. In 2014, Macey et al. (2014) developed a community-based experiment to measure volatile organic compounds (VOCs) concentrations near an oil and gas production site. In their experiment, grab and passive air samples were collected by trained volunteers at locations identified through systematic observation of industrial operations and air impacts over the course of residents' daily routines. A total of 75 VOCs were measured using EPA Method TO-15 or TO-3 by gas chromatography/mass spectrometry. Formaldehyde levels were determined using UMEx 100 Passive Samplers. The result revealed that the levels of eight VOCs exceeded federal guidelines under several operational circumstances. Benzene, formaldehyde, and hydrogen sulfide were the most common compounds to exceed acute and other health-based risk levels (Macey, et al., 2014).

1.2. Sensors and Microcontroller for Air Monitoring

The use of microcontrollers in air monitoring systems has increased significantly. The readily availability of cheap, low-power demanding, and miniature embedded processors, radios, sensors and actuators, often integrated on a single chip, is leading to the rapid development of portable air monitors and distributed monitoring networks. In addition to air quality sensors, other sensors that are useful for instrumentation (monitors and monitor networks) development include seismic, magnetic, thermal, visual, infrared, acoustic and radar sensors. Nowadays, even a simple air monitoring system may require an integration of various electronic and pneumatic components: microcontroller, gas sensors, GPS/GPRS module, data transceiver, current regulator circuit, ADC (analog-to-digital converter) and LED indicators (Al-Haija, Al-Qadeeb, & Al-Lwaimi, 2013).

Gas and other sensors that can be easily interfaced with microcontrollers have been improved significantly; and they have become more capable, economical and reliable than ever before. For example, in a 2008 report, Kularatna and Sudantha compared the characteristics of regular gas sensors and modern semiconductor gas sensors. A gas sensor is a transducer that detects gas molecules and produces an electrical signal with a magnitude proportional to the concentration of the gas. Modern semiconductor gas sensors are capable of detecting more than 150 different gases. They have many advantages including but not limited to longer lifetime than catalytic bead and electrochemical sensors, lower cost, and compact size. These sensors are widely used in various applications: automotive, consumer, commercial, industrial, indoor and outdoor air quality monitoring, and environmental monitoring (Kularatna & Sudantha, 2008). A semiconductor sensor consists of one or more metal oxides such as tin oxide and aluminum oxide. When heated to a high temperature, an n-type semiconductor material decreases its resistance, while p-type increases the resistance in the presence of a reducing gas (Capteur

Sensors, 2000). Typically, a semiconductor sensor produces a strong signal, especially at high gas concentrations with adequate sensitivity, fast response time, long-term stability, and longer lifetime. However, the sensitivity of most semiconductor sensors is, at the current stage, poorer than that of regular gas sensors, which impedes the application of semiconductor sensors to ambient air quality monitoring.

Microcontrollers have been used in many projects associated with air quality monitoring. In 2013, Al-Haija and his colleagues developed a microcontroller-based air monitoring system to measure air quality at King Faisal University. Their design included several units: Arduino Microcontroller, MQ-2 Gas Sensors, and the current regulator circuit; and was enhanced with Wireless Sensor Network (WSN). As a result, it can provide a real-time information about the level of air pollution in different regions, as well as provide alerts in cases of drastic change in air quality. In their conclusions, they pointed out that the design can be enhanced by several ways such as: adding a wireless network card to the microcontroller circuit for better and easier control of the sensor readings as well as more sophisticated sensors could be used such as MQ-135 and MQ-136. Their project demonstrated that microcontrollers are more than capable of doing air monitoring work and measuring the level of gaseous pollutants in the air such as hydrogen (H_2S), ammonia (NH_3), alcohol and others (Al-Haija, Al-Qadeeb, & Al-Lwaimi, 2013).

In another paper written by Shrivastava and his colleagues (2013), the authors generalized the working principle of any microcontroller-based monitoring system. They stated that the operation of all existing air monitoring systems involved three steps. In the initial step, the target gaseous pollutant is detected by a gas sensor or sensor array. The sensor then sends a detection signal to the microcontroller via a specific communication protocol. In the second step,

the microcontroller receives the signal sent by the gas sensor and based on a comparison of the signal with a pre-set criterion it may send control signals to other external devices to manipulate their operation. In the last step, monitoring data is delivered to users and this may include buzzing, displaying messages on a liquid crystal display (LCA) screen, and sending warning SMS to remote users via GSM or WIFI network (Shrivastava, Prabhaker, Kumar, & Verma, 2013).

1.3. UAV Systems

An unmanned aerial vehicle (UAV), commonly known as a drone, is an aircraft without a human pilot aboard. UAVs are a component of an unmanned aircraft system (UAS); which include a UAV, a ground-based controller, and a system of communications between the two. In practice, the terms UAV and UAS are often interchangeably used. The flight of UAVs may operate with various degrees of autonomy: either under remote control by a human operator or autonomously by onboard computers (International Civil Aviation Organization, 2016).

UAV-based monitoring is extremely popular in recent years due to the rapid growth of technology in drones. In the paper "Unmanned Aircraft Systems in Remote Sensing and Scientific Research: Classification and Considerations of Use," Adam Watts and his colleagues explained how airborne monitoring with UAVs is possible, and the advantages of such systems. Airborne monitoring refers to reconnaissance techniques using aircraft, UAV, or other platforms. UAV has four main advantages over remote sensing: relatively low cost, flexibility in the frequency and time of data acquisition, and the ability to record finer spatial details than the current satellite technology. The UAV monitoring system is based on UAV which has both the common characteristics of aerial monitoring and its own unique features. Compared with manned aerial vehicles, monitoring systems with the platform of UAV can work all-day and all-

weather and perform flight tasks in high-risk areas. Moreover, UAVs are able to operate rather close to the object and acquire images with a resolution at few centimeters, providing sufficient details. With the development of sensors and communication techniques, high-resolution airborne monitoring has been successfully applied to large-scale topographic mapping and surveying for detailed ground information. Although existing airborne monitoring has some drawbacks, such as altitude, endurance, attitude control, all-weather operations, and monitoring of the dynamics, it is still an important technique of studying and exploring the Earth's resources and environment (Watts, Ambrosia, & Hinkley, 2012).

The biggest challenge to UAV-based monitoring systems is communication with the ground station. In the paper "A UAV Remote Sensing System: Design and Tests" written by Yan et al. (2009), this problem has been explained and addressed. The authors believe that even though the UAV can fly automatically under the control of the pre-set program, it should preferably be always controlled and monitored from the Ground Control Station, so it needs reliable communication that links to and from the aircraft. The Ground Control Station provides a working space for a pilot, navigator, instrument operator and usually a mission commander. The onboard sensors are controlled by the airborne control system to capture images or do other measurements of the working area. After basic and real-time processing on board, the data can be downloaded to the Ground Control Station for on-site processing or forwarded to a processing center. The data processing center or ground receiving station will then further process, archive, manage and distribute the data for expert users. Advanced processing may involve information extraction and application. In this way, the operation of the UAV monitoring system is accomplished, and a complete set of protocols and standards can be realized (Yan, Gou, & Duan, 2009).

Chapter 2

This chapter describes our efforts to design, fabricate and test a UAV-based air monitoring system, and to apply this system to a few field trials. This section is prepared as a journal manuscript and therefore will include some redundant information that has been presented in Chapter 1.

2. Development of a UAV-Based System for Monitoring of CH_4 and CO_2 over an Oil Field

2.1. Introduction

Horizontal drilling and hydraulic fracturing, which enable one to tap tight rock formations, are a crucial component of the recent boom of shale gas and oil production in Northern America. Besides their inherent economic advantages, these unconventional energy technologies represent a potential opportunity to reduce greenhouse gas emissions because the combustion of natural gas or oil produces less carbon dioxide (CO_2) per unit of energy than that of coal (by ~56% for gas and ~79% for oil) (U.S. Energy Information Administration, 2011).

A significant amount of methane (CH_4) is emitted from well completion during unconventional gas and oil production (Howarth, Santoro, & Ingraffea, 2011). CH_4 is a potent greenhouse gas with its global warming potential (GWP) 25 times higher than that of CO_2 over a 100-year time horizon (Intergovernmental Panel on Climate Change, 2007). CH_4 emissions occur when the fracturing fluid, which is injected into the dense, nonporous medium at high pressures to create fissures in the shale, flows back to the ground surface; and when the plugs that separated the sections of the fracturing stages of the well being drilled out. In the production process of tight oil, co-occurring natural gas is typically used to drive the oil to the wellbore (U.S. Energy Information Administration, 2012), which also leads to the release of CH_4 to the atmosphere. As the productivity of unconventional wells is initially high but depletes rapidly,

new wells are continuously being drilled. CH_4 emissions from field production of oil and gas from tight reservoirs may reverse the climate impact mitigation, at least in the short run, if the leakage rate exceeds the break-even point. Mitigating the environmental impact of oil and gas activities is extremely important to the oil and gas industries.

Sources of variability in aerial concentrations and emissions of methane, volatile organic compounds (VOCs) and other pollutants near unconventional oil and gas (UOG) sites include: (1) the spatial variability in UOG operations; (2) the discontinuous use of equipment such as diesel trucks, glycol dehydrators, separators, and compressors during preparation, drilling, hydraulic fracturing, well completion, and other stages; (3) the composition of shale and other formations and the specific constituents of the drilling and hydraulic fracturing fluids used on-site (which can influence the makeup of produced or flowback water stored in pits and tanks); (4) intermittent emissions from venting, flaring, and leaks; (5) the shifting location, spacing, and intensity of well pads in response to market conditions, improvements in technology, and regulatory changes; (6) the effects of wind, complex terrain, and microclimates; and (7) considerable differences among states in permitting, leak detection and repair, and other requirements (Macey, et al., 2014).

The oil and gas industry has a variety of effective tools available for estimating the emissions of hydrocarbons from point sources associated with major processing units. These include: GRI-GLYCalc® for estimation of emissions from glycol dehydration units; API E&P Tank® model for flashing emissions from storage tanks; process simulators such as HYSIM® and HYSIS® that are used to estimate the emissions from various production and processing unit operations; and direct measurement (Hashmonay & Ramsey, 2018).

The use of unmanned aerial vehicles (UAVs) for air quality assessment is rapidly growing. Their ease of deployment and high maneuverability allow them to sample areas otherwise inaccessible with conventional platforms. For example, suborbital research aircraft with onboard pilots do not fly over populated areas at low altitudes, volcanoes, or into severe weather for safety reasons (Khan, et al., 2012). Tethered balloons and kites can provide vertical resolution measurements but only over a single location, and their deployment is limited to specific weather conditions. UAV platforms have also demonstrated promise for atmospheric chemistry field studies. Substantial payloads are now routinely lifted by unmanned aerial vehicles, particularly for real-time monitoring.

This study aims to construct a functional system that could be used at petroleum and natural gas production sites to monitor methane emissions as well as other releases. The specific objectives of this project are to:

- Design and construct a UAV-based air monitoring system;

- Build a wireless communication system that sends real-time monitoring data to a ground station;

- Perform field air monitoring using the constructed UAV-based system.

The two main air pollutants that were investigated were CH_4 and CO_2 because significant emissions of these pollutants are commonly found over oil and gas fields.

2.2. System Description

2.2.1. Functional Overview

The UAV-based air monitoring system (UBAMS) designed for this project consisted of several parts: gas sensors, a LoRa wireless transmission module, a microcontroller, a GPS module, and an SD card shield. The gas sensors included CH_4 and CO_2 sensors. A temperature

and humidity sensor was used to correct for CH$_4$ sensor readings. The GPS module provided the

physical coordinate location of the monitoring unit, as well as time and date in National Marine

Electronics Association (NMEA) format. The microcontroller coordinated the operation of

sensors and other devices. The Long-Range radio service (LoRa) module transmitted the

monitoring data, including time, date, physical location, and the concentration level of air

pollutants, to a ground station.

The schematic diagram of the air monitoring system is shown in Figure 1. All the sensors

including the GPS and LoRa modules were connected to the microcontroller. The assembly was

mounted on a drone. A rechargeable battery was used to power the operation of the sensors

during field data collection. Data was collected and saved to external storage (a microSD card).

The data was also sent to the ground station via a wireless module.
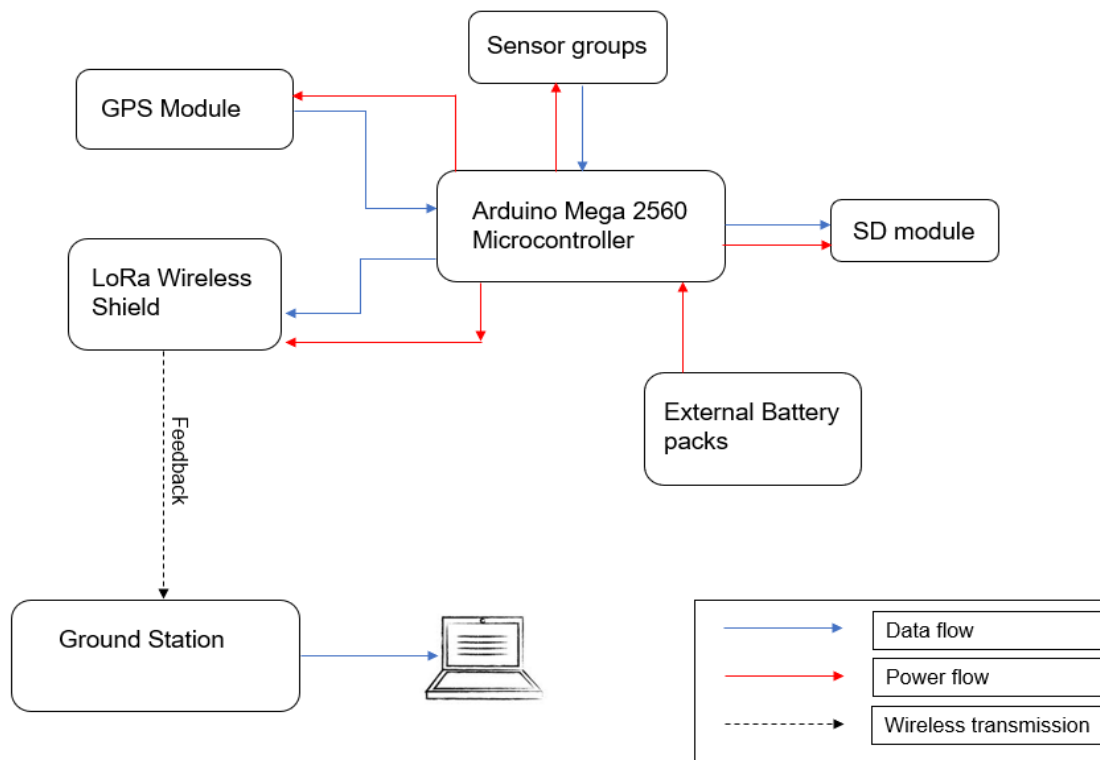
Figure 1: Schematic diagram of the air monitoring system

A graphic user interface (GUI) created with NI LabVIEW was applied to the ground station. While the pilot is operating the UAV, the ground station receives the data, and the data is transformed into a more intuitive format to display on a laptop. Figure 2 demonstrates the overall functionality of the hardware developed for the project:
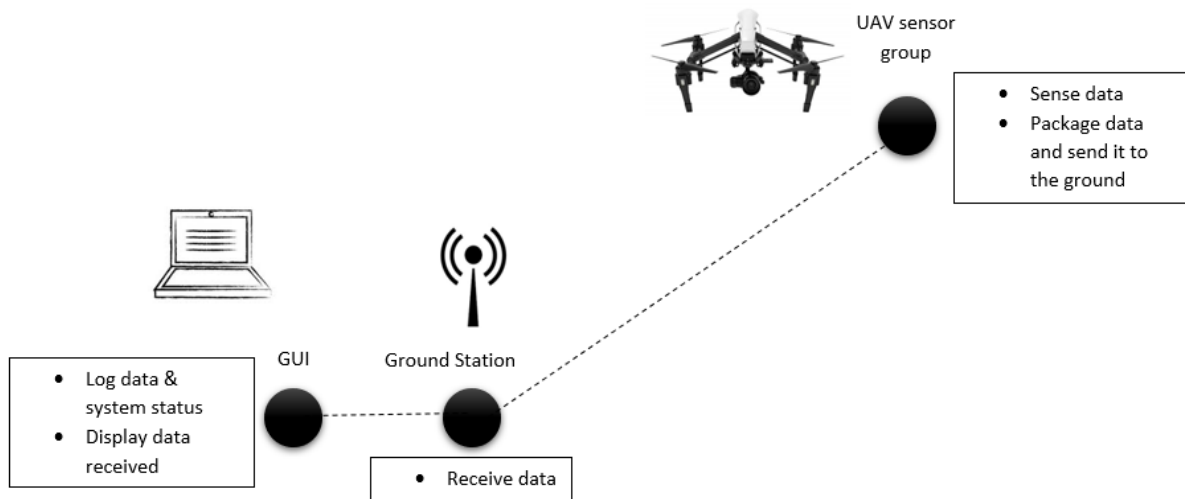
Figure 2: Functionality of the air monitoring system

2.2.2. Airborne Sensor Node

In this project, an Arduino Mega microcontroller was used for sensor control and data collection, data logging, and communication, serving as the "central commander" of the airborne sensor node. The microcontroller was coded to achieve the desired functionality using the Arduino programming language (which is based on C/C++).

Figure 3: Arduino Mega 2560 microcontroller

Arduino is an open-source computer hardware and software platform. It consists of both a physical programmable board (as known as microcontroller) and an Integrated Development Environment (IDE) that runs on a personal computer. The Arduino does not require any additional hardware to load codes onto the board, and its simple programming syntax makes it very easy to use (B_E_N, 2018).

The Arduino Mega (Figure 3) is a microcontroller board based on the ATmega1280 chip. It has 54 digital input/output pins (14 of which can be used as PWM outputs), 16 analog inputs, 4 UARTs (hardware serial ports), a 16 MHz crystal oscillator, a USB connection, a power jack, an ICSP header, and a reset button (Arduino Mega, 2018). With its capabilities, the Arduino Mega board is widely used for prototype product development. Figure 4 shows a schematic diagram of a typical Arduino Mega board.
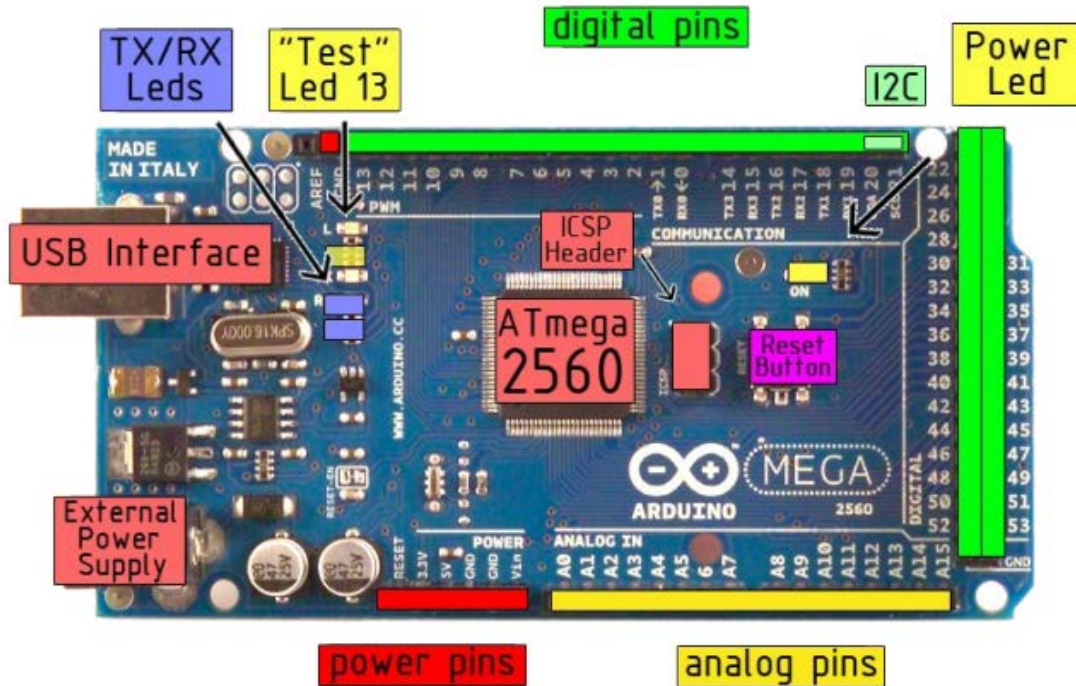
Figure 4: Arduino Mega 2560 schematic diagram (Arduino Mega, 2018)

The main components of this design were the gas sensors. There were three sensors used for this project: a CO_2 sensor, a CH_4 sensor and a temperature/relative humidity sensor. These sensors, upon exposure to open air, collect the concentration of pollutants and send the data to the microcontroller. Other pollutant gases and gas sensors are not considered in this study. However, a minor revision of the code would allow them to be incorporated to the existing system.

An MH-Z14A CO_2 sensor (Figure 5) uses the non-dispersive infrared (NDIR) principle. It measures CO_2 up to 5000 ppm with a deviation of $\pm10\%$ of reading value ($\pm3\%$ of reading value from 0-5000 ppm). The sensor sends the CO_2 signal in three output modes: digital serial output (RS-232), analog voltage signal, or PWM (Pulse Width Modulation). For this project, the serial output was selected.
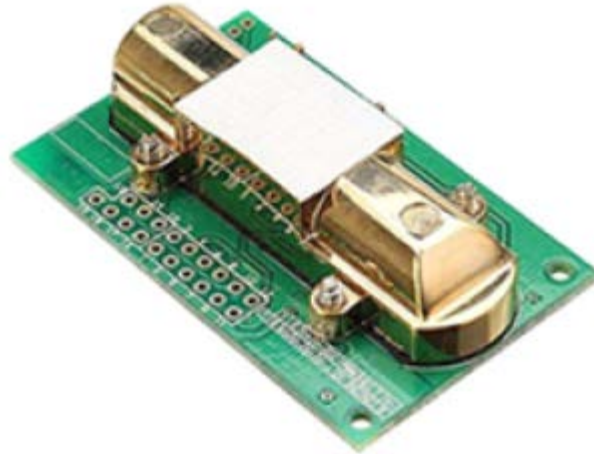
Figure 5: MH-Z14A CO$_2$ sensor

A TGS 2600 sensor (Figure 6) is a low-power-consumption but high-sensitivity sensor that can detect a wide range of air pollutants, including CH$_4$. The sensor is a metal oxide semiconductor sensor. Inside the sensor, a metal plate reacts with the pollutants, resulting in a change in conductivity and accordingly the output voltage. The sensor uses only analog output (0-5V). According to a previous study (Eugster and Kling, 2012), it can measure CH$_4$ concentrations as low as 1.8 ppm, the background CH$_4$ concentration in the atmosphere.

Figure 6: TGS 2600 methane sensor

Since TGS 2600 can only provide a raw analog signal output, calibration is needed to translate this raw signal into actual CH4 concentration reading. Eugster and Kling (2012) developed a step-by-step instruction to calculate the CH4 concentration from the sensor's analog output. Initially, the sensor has a certain resistance R_0 in clean air, which is reduced with the presence of a target gas. This reduced resistance R_s can be expressed by a power function:

$$R_S = A[C]^{-\alpha}$$
(1)

where R_s is the actual sensor resistance, A is a coefficient for the gas at concentration [C], and α is the slope of the curve as shown in Figure 7:
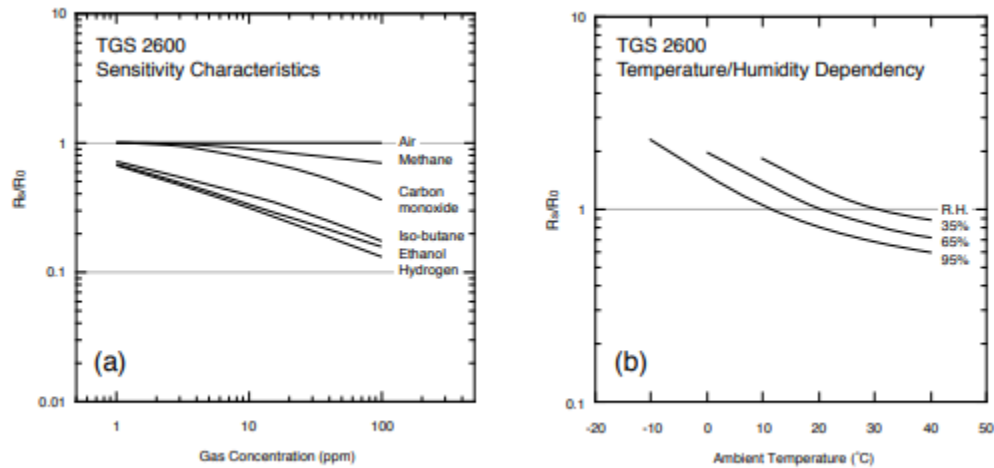
Figure 7: TGS 2600 sensor response (a) and sensitivity to temperature and relative humidity (b) according to manufacturer specifications.

where R_s/R_0 is the ratio between sensor resistance (R_s) under the presence of a specific component in relation to the reference resistance (R_0) in "fresh" air without any of the additional chemical components. The sensor resistance can be determined as:

$$R_S = \frac{V_c * R_L}{V_{out}} - R_L$$
(2)

where V_c is the supply voltage of 5.0 VDC, and V_{out} is the voltage measured over the precision resistor R_L. R_L was set to 2.5 kΩ in this study. To address the impact of temperature and humidity on sensor response, the following equation was used:

$$\left(\frac{R_S}{R_0}\right)_{corr} = \frac{R_S}{R_0} * (0.24 + 0.0072 * RH + 0.0246 * T_a) \tag{3}$$

where RH is relative humidity in percent, and T_a is air temperature in °C. Finally, CH4 concentration can be calculated as (Eugster & Kling, 2012):

$$[CH_4] = 1.8 + \frac{0.1}{\left(\frac{R_S}{R_0}\right)_{corr}} \tag{4}$$

The DHT22 temperature and humidity sensor (Figure 8) uses a polymer capacitor as the sensing element, which is capable of operating in 0-100% relative humidity and -40~80 °C. This sensor sends digital signals to the Arduino Mega board via a serial connection (RS-232). The temperature and humidity data was used to correct for the R_S/R_0 value in equation 3.

Figure 8: DHT22 Temperature and humidity sensor

A Ublox NEO-6M GPS module (Figure 9) was used to provide the physical coordinate location of the monitoring unit, as well as time and date to the user. This unit is a stand-alone

GPS module with 50 channels and a 6-positioning engine. The unit is equipped with a 25x25 mm patch antenna and it uses digital serial output only.

Figure 9: NEO-6M GPS module

To avoid the loss of important data during monitoring due to a weak wireless signal, an SD card shield (Figure 10) was used to back up the data. The shield uses the SPI bus to transfer data from the microcontroller to a standard SD card, and vice versa.
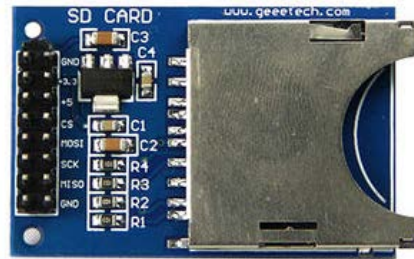
Figure 10: Arduino SD card shield

2.2.3. LoRa Wireless Modules

Long-Range communication (LoRa) is considered one of the most promising wireless communication protocols for the Internet of Things (IoT) applications, including distributed air monitoring. The technology employs a spreading technique, in which a symbol is encoded in a

longer-than-essential sequence of bits, thus reducing the signal-to-noise ratio required at the
receiver for correct reception without changing the frequency bandwidth of the wireless signal.
The length of the spreading code can be varied, thus making it possible to provide variable data
rates and a possibility to trade throughput for coverage range, or link robustness, or energy
consumption. It uses license-free sub-gigahertz radio frequency bands such as 433 MHz, 868
MHz in Europe and 915 MHz North America due to regulations (Centenaro, Vangelista, Zanella,
& Zorzi, 2016).

The LoRa network (LoRaWAN) consists of end nodes, gateways/concentrators, and
network controllers. Although the long-term goal is to build a LoRawan to send real-time
monitoring data from multiple UAVs to a web server, in this study the LoRa modules were
configured to enable a point-to-point communication (i.e., UAV to ground station).

The Dragino LoRa module (Figure 11) was used in this project. The module is physically
compatible with the Arduino Mega board. It uses the SPI bus to communicate with the
microcontroller, and the frequency band it uses was pre-configured at 915 MHz.
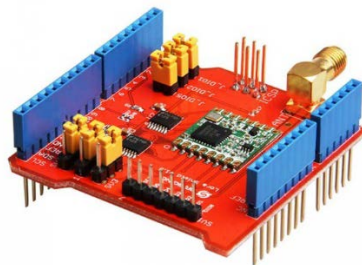
Figure 11: Dragino LoRa Module

2.2.4. Ground Station and Graphic User Interface

The primary function of the ground station is to receive data and then transfer the data to
a laptop. The structure of the ground station is elementary, with a Dragino LoRa module attached

to an Arduino Uno board. This provides good communication with a tested maximum communication distance of 800 meters. This setup was coded with Arduino as well.

The National Instruments (NI) LabVIEW was used to create a graphic user interface (GUI) on the laptop. The GUI (Figure 12) allows one to easily manage, save and visualize the real-time data. A LabVIEW application (.EXE) was created and it can run on any computer that has the LabVIEW run-time environment and NI-VISA driver installed.
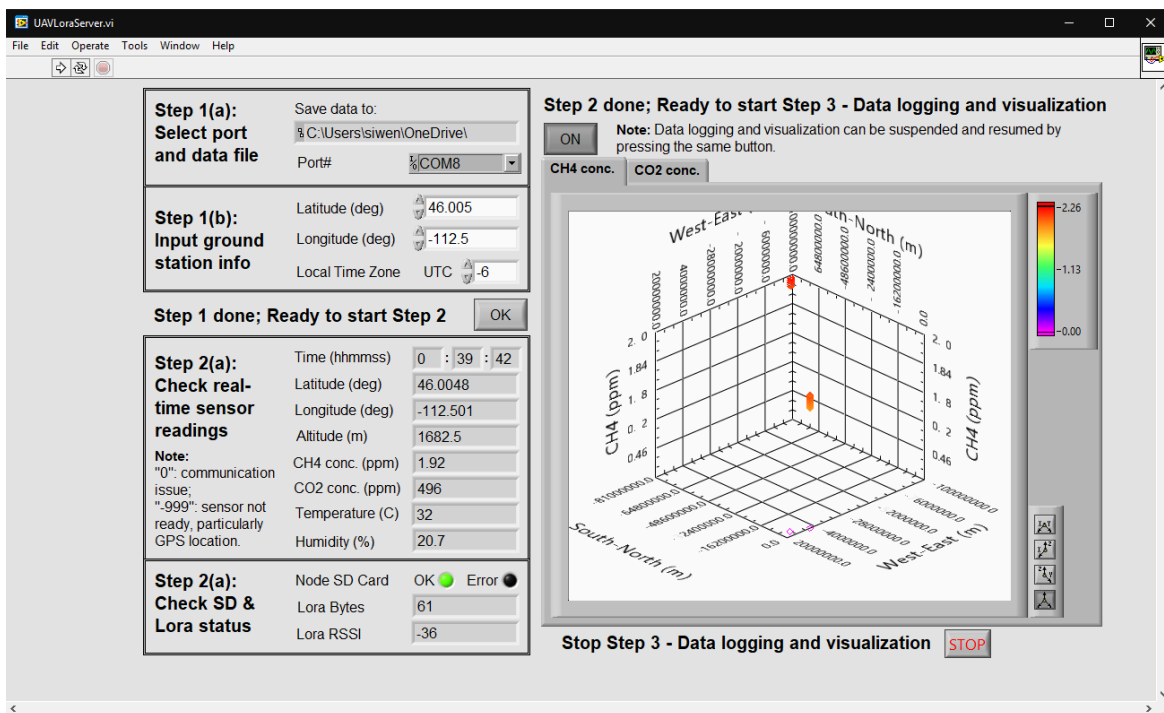
Figure 12: NI LabVIEW Graphic User Interface

2.2.5. System Assembly

To support the designed system, the choice of UAV must be discrete to avoid any potential accidents. For this project, a DJI Inspire 1 V2.0 (Figure 13) was selected because of its ruggedness. The maximum payload of the DJI Inspire 1 is up to 1 kg. Under load, the drone can

reach 15 m/s of maximum flight speed and a total of 15 minutes flight duration. Therefore, it is well suited for this study.

Figure 13: DJI Inspire 1 V2.0

Autodesk Fusion was used to create the 3d model of enclosures (Figure 14) for the sensor node and the ground station. Since the UAV can only support 1 kg of payload, a light but sturdy enclosure is a must. Accordingly, the enclosures were 3-D printed with ABS plastics. With the enclosure, the total weight of the airborne sensor node was under 500 grams. The enclosure also includes multiple I/O ports for various uses, as well as air vents for gas sensors.
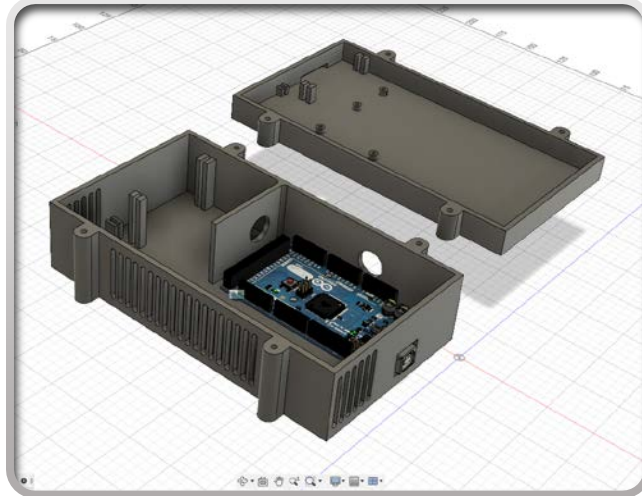
Figure 14: 3D model of the enclosures for the airborne sensor node

The prototype system was fabricated and assembled in early October 2018. Figure 15 shows the final product. On the left is the airborne sensor node that houses all the necessary sensors and modules. This unit was attached to the UAV. A removable battery was attached on the top of the unit, as well as some hinges for connecting to a UAV. On the right is the ground station. The receiver was connected to a personal computer at ground station via a USB cable. Figures 16 and 17 show the interior of the airborne sensor node.
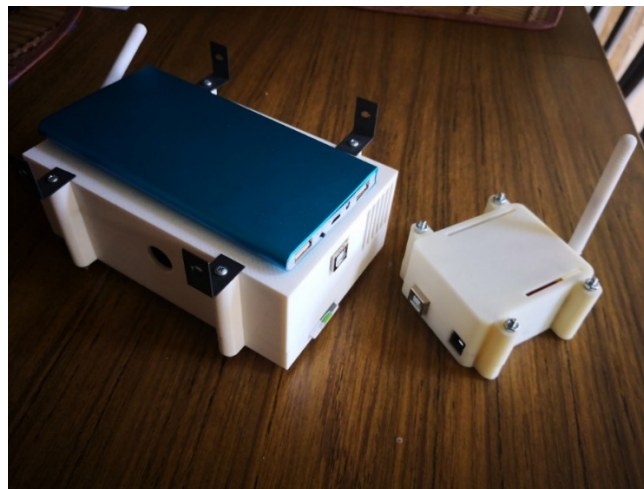
Figure 15: Finished prototype monitoring system
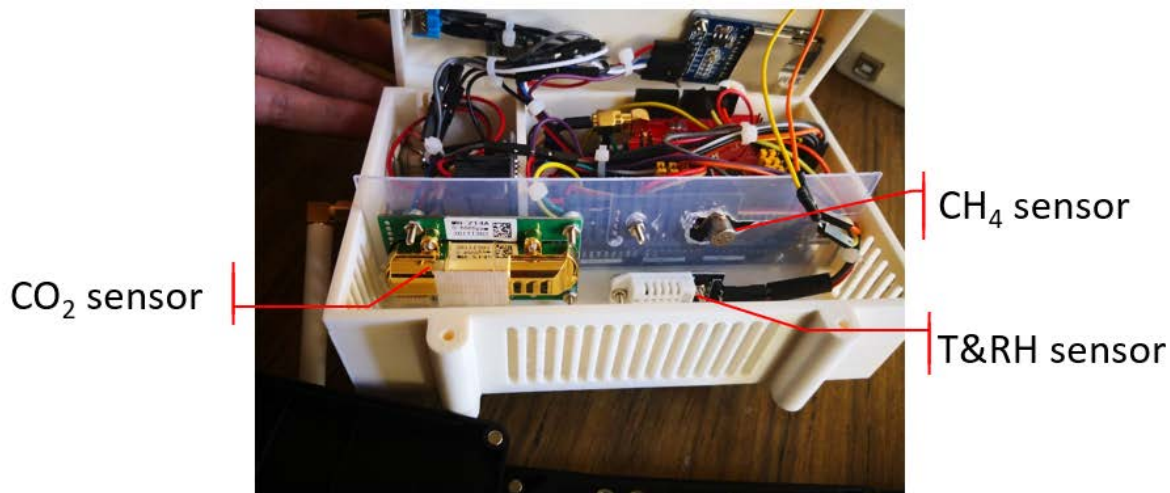
Figure 16: Interior of the airborne sensor node: side view
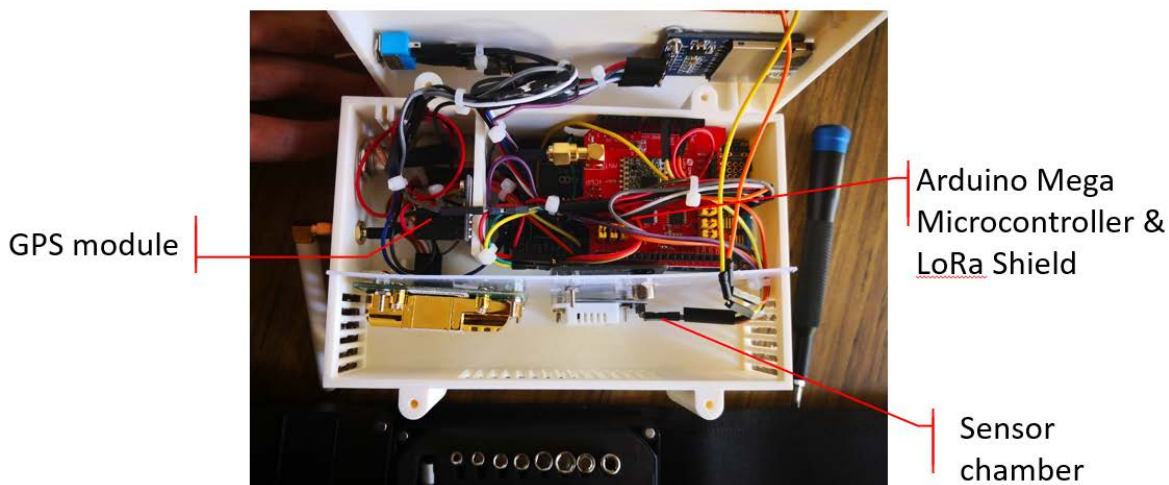
Figure 17: Interior of the airborne sensor node: top view

All the gas sensors were arranged in the same chamber. The gas chamber had multiple vents on each side of the chamber to offer air flows during operation. The sensors were fixed on a piece of removable plastic plate. This structure makes it easier to fix or replace when maintenance is needed. On the top right were the Arduino Mega microcontroller and LoRa module. The GPS module and an extended LoRa antenna were fixed to the top left corner.

During operation, the GPS antenna faced upward while the LoRa antenna faced downward to maximize the signal strength. An SD card was inserted through a slot on the side of the enclosure. An additional DC power jack and a power switch were placed on top of the unit as well.

As shown in Figure 18, the airborne sensor node was connected to the UAV using copper wires. This setup ensured the flight stability and security while operating. Overall the design was successful. Each component was securely assembled without any additional modifications. All components in this unit functioned as expected.
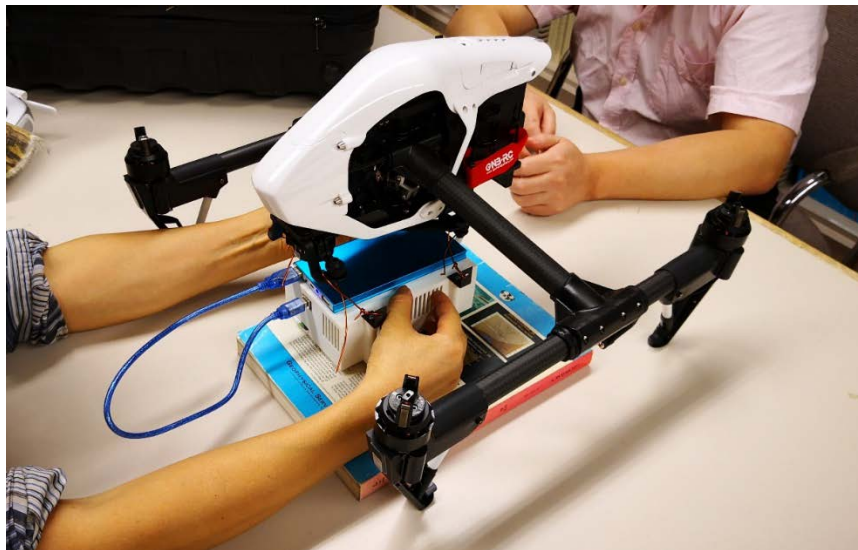
Figure 18: Mounting the airborne sensor node to a UAV

2.3. Experiments and Results

2.3.1. Preliminary Trial

The preliminary test was performed in early October 2018. The test was conducted in Butte, MT, roughly 1 mile west of Montana Tech Campus because of its ease of access and deployment. The purpose of this preliminary trial is to determine the system's responsiveness, stability, and communication with the ground station. The UAV's pilot was also trained during the test to develop the necessary skills to operate the UAV.

The system was found to be very responsive. The data transmission between the UAV monitoring system and the ground station was seamless. The data transmission was stable and smooth with no visually noticeable lags, which makes it close to "real-time" communication. The system was also robust. Despite the windy condition and the extra weight, the UAV did not have any trouble with taking off, flying and landing. It was also noted that the wireless signal from the airborne sensor node was strong, to within approximately 800 meters, which is reasonable given the LoRa RF configuration set on the ground station.

2.3.2. Field Test

The field tests were performed in early November 2018. The Williston Basin was selected for the tests because of its richness in petroleum and coal bed methane deposition. The Williston basin lies on western North Dakota, eastern Montana, and southern Saskatchewan. This basin makes North Dakota the second largest oil-producing state in America (Walton, 2015). Most of the crude oils in North Dakota also contain some natural gas, and most of the natural gas produced in North Dakota is "wet gas," that is, it contains hydrocarbons that are liquid under pressure but a gas at surface pressures (Overview of the Petroleum Geology of the North Dakota Williston Basin, 2018). The rich carbonate deposition makes the Willison Basin an

ideal choice for the test – as, theoretically, the methane concentration in the atmosphere could be higher in this region.

The well sites tested are approximately 30 miles east of Sydney, MT and 8 miles south of Alexander, ND. Two wells were tested during the testing day. These two wells are about 1 mile away from each other. Figure 19 is a top view of these two wells in a Google Earth image.

Figure 19: Plan view of the well sites on Google Earth

These two wells are located on a flatland close to a major highway. Busy traffic was noted during the field test. Also noted were the weather conditions. During the testing period, the ambient temperature was about 15 °F with moderate to high wind speeds (about 10 mph). Light precipitation also occurred during the testing period. These factors were believed to have influences on the gas distribution and diffusion; thus it might affect the outcome data. Figure 20 is an aerial view of the well shot with the UAV. Note the gas flare location circled in red. Higher concentrations of pollutant gas were expected around that spot.

Figure 20: Plan view of the well sites by using the UAV

2.3.3. Post-Field Test Data Analysis

A total of four tests was performed during the field campaign. Three of the four tests were performed around well #1, and the fourth test was performed around well #2. Thus, a total of four sets of data were collected. The data sets were later processed with Oasis Montaj to generate colored contour plots. Both the raw data and the colored contour plots are discussed in this section.

The data collected was transferred to Oasis Montaj for more in-depth analysis. Oasis Montaj is a software developed by GEOSOFT that is capable of drawing contour plots with given geology information. Oasis Montaj provides a powerful way of visualizing data, and it allows the visualized data to be displayed on Google Earth with its built-in map creator. This gives a much more intuitive way of comparing results.

The purpose of the first trial was to finalize the flight path and estimate the potential hazard during flight. In this case, the sampling spots were not as uniformly distributed as other trials. By looking at the raw data, the changes in both CH_4 and CO_2 were not significant. Gas concentrations appeared to be relatively constant throughout the area, and no predictions could be made at this point. The Oasis Montaj contour maps provided an intuitive view of changes in concentrations in this case. Figure 21 shows a map of distributed CH_4 concentrations. It is important to note that the scale was in relative concentration.
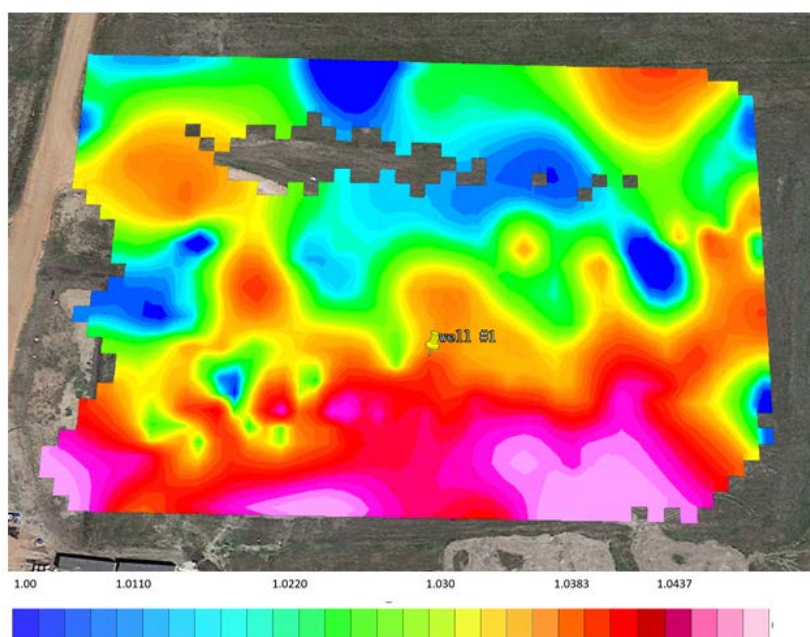
Figure 21: Contour plot of CH₄ relative concentrations from trial #1

This intuitive map clearly shows that CH_4 concentration was higher in the lower regions of the well site. Figure 22 shows a Google earth image of the well. Note the peak of the concentration is around the gas flare circled in red.

Figure 22: Google Earth image of well #1

By comparing Figure 21 and Figure 22 one can see that the methane concentration was higher around the gas flares. Some unburned natural gas might have escaped, which is commonly found over an oil field. Figure 23 shows a contour plot of CO_2 concentrations during the same trial.

Here, the CO_2 concentration is increasing at the north of the well site possible caused by the traffic on the highway. Higher CO_2 emissions are expected during a high volume of traffic. Overall, this model has successfully reflected the distribution of the CH_4 and CO_2 concentrations around this well site.
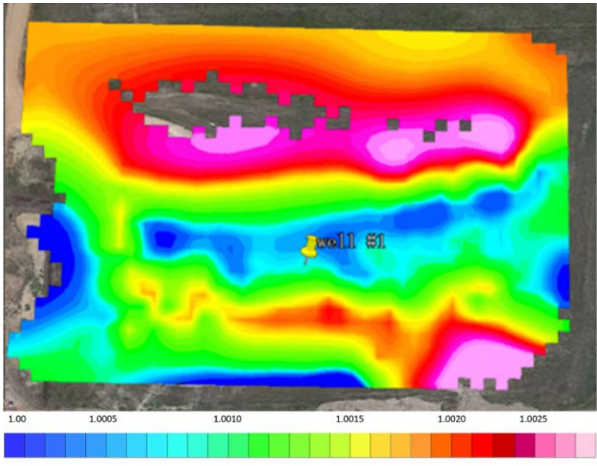
Figure 23: Contour plot of CO_2 relative concentrations from trial #1

The second trial was performed at the same location but a relatively lower elevation (20 meters AGL). Like the first trial, raw data did not show much of a difference. Colored contour maps were created for comparison. Figures 24 and 25 are the Oasis Montaj contour maps developed from CO_2 and CH_4 concentrations, respectively.
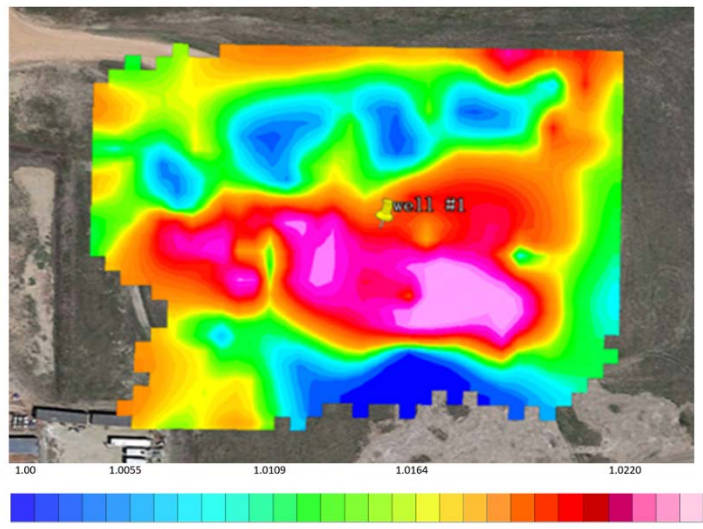
Figure 24: Contour plot of CH4 relative concentrations from trial #2
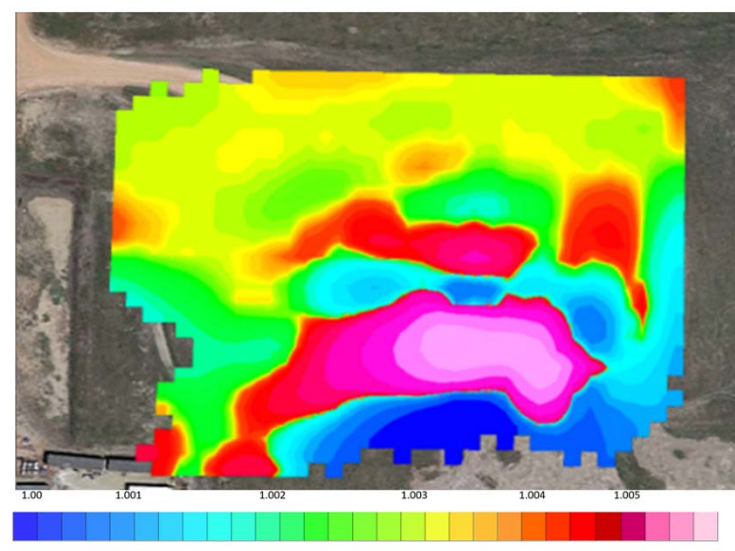
Figure 25: Contour plot of CH4 relative concentrations from trial #2

Like the first trial, both the CO_2 and CH_4 concentration were relatively higher around the gas flare. Unlike the first map, this map appeared to be more uniform regarding gas distribution. The next model proves this hypothesis. The third trial was performed at a higher elevation (45 meters AGL). Figures 26 and 27 showed the CH_4 and CO_2 distribution modeled by Oasis Montaj, respectively.
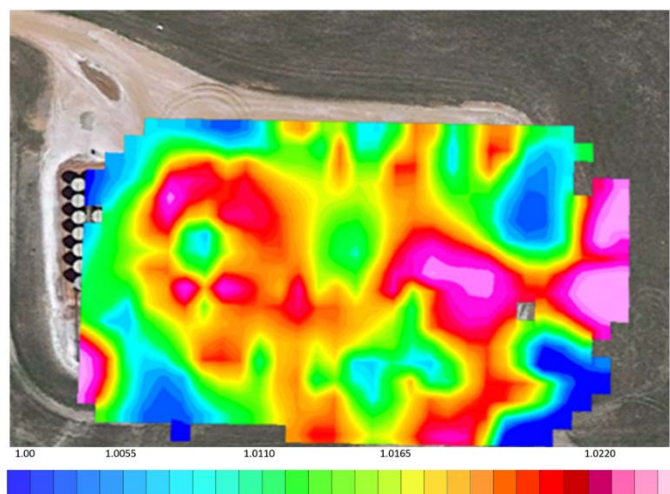
Figure 26: Contour plot of CH₄ relative concentrations from trial #3
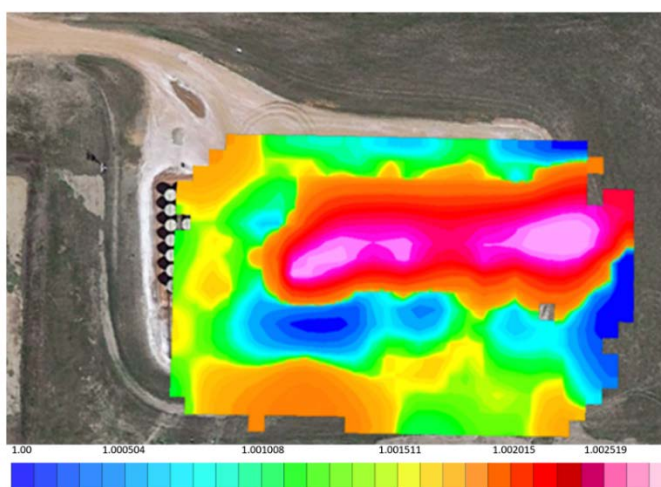
Figure 27: Contour plot of CH₄ relative concentrations from trial #3

At a higher elevation, diffusion was observed. The CH_4 concentrations were significantly lower; while the area with peak CO_2 concentration was shifted northwards. The map also showed that the concentrations of both CH_4 and CO_2 were still relatively higher around the gas flare. Figure 28 provides a comparison of CH_4 and CO_2 distribution at different elevations. Overall CH_4 and CO_2 concentrations tended to decrease with altitude. Two of the factors that may explain this trend are high wind speeds and changing wind directions.
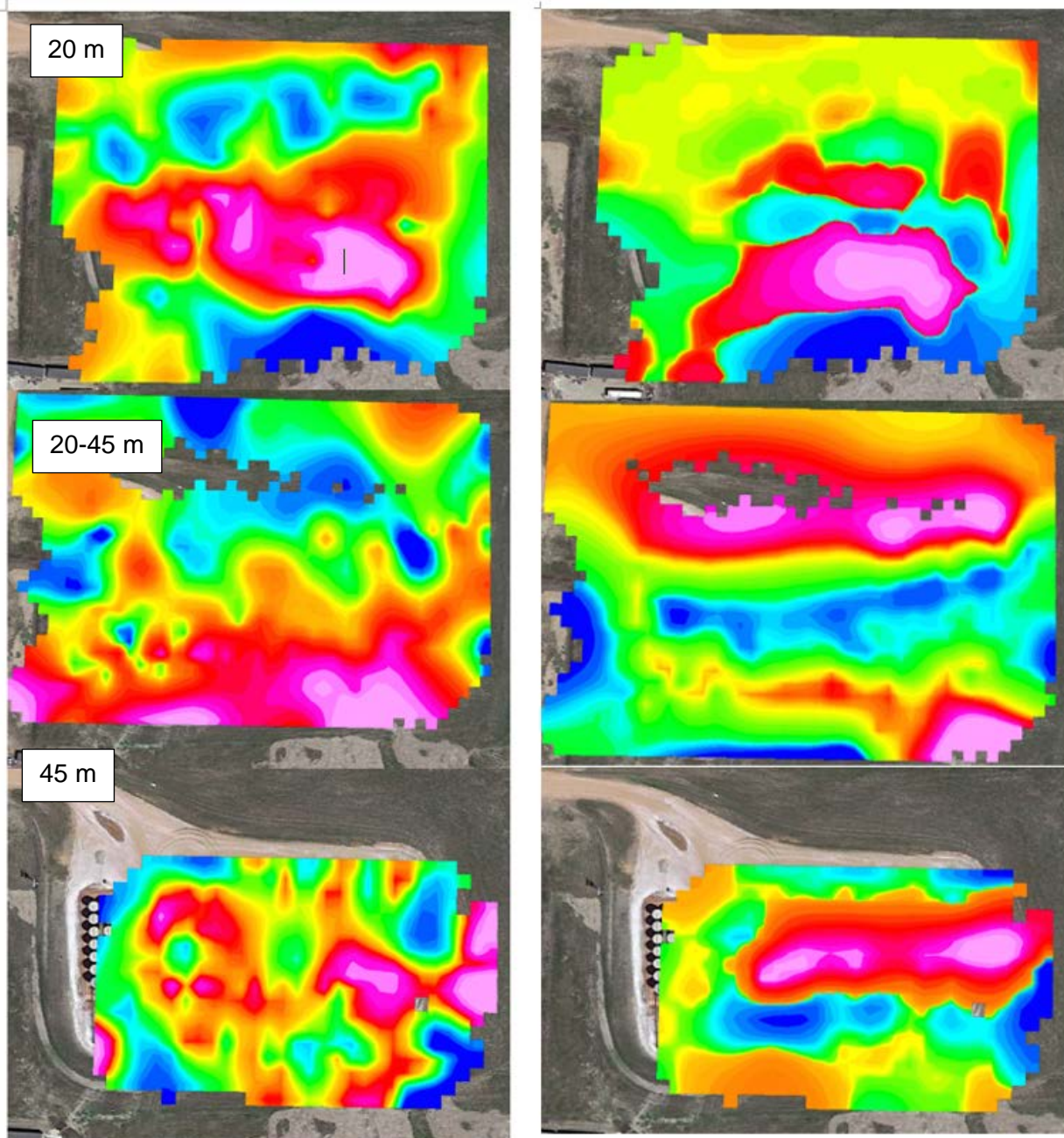
Figure 28: Gas concentration/distribution versus elevation: (left) CH_4 and (right) CO_2

The fourth trial was performed on a different well location. It is worth noting that the gas flare was shut off at this well site. No definite conclusion was drawn from data analysis. The changes in CH_4 or CO_2 concentrations were not distinct. A Google Earth image of the well site and the contour plots of CH_4 and CO_2 concentrations are given in Figures 29, 30 and 31.

Figure 29: Google Earth image of well #2

| 1.00 | 1.00550 | 1.0100 | 1.0220 | 1.0275 | 1.0330 |
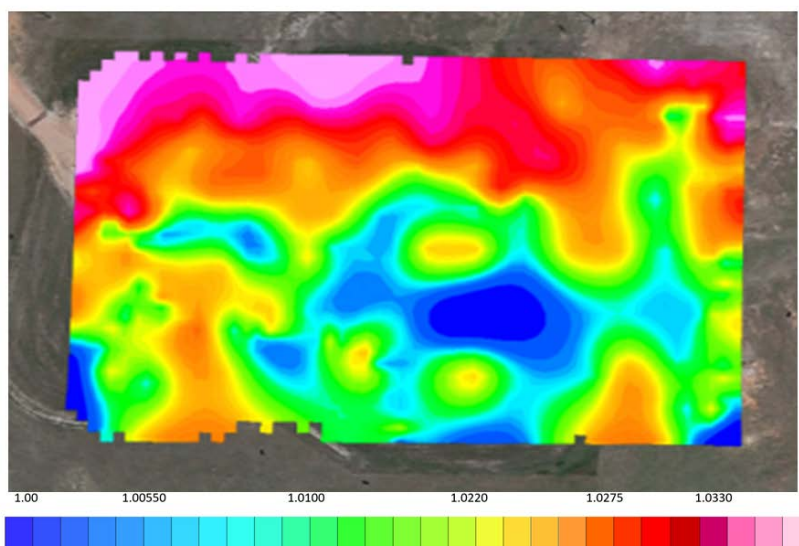
Figure 30: Contour plot of CH$_4$ relative concentrations from trial #4
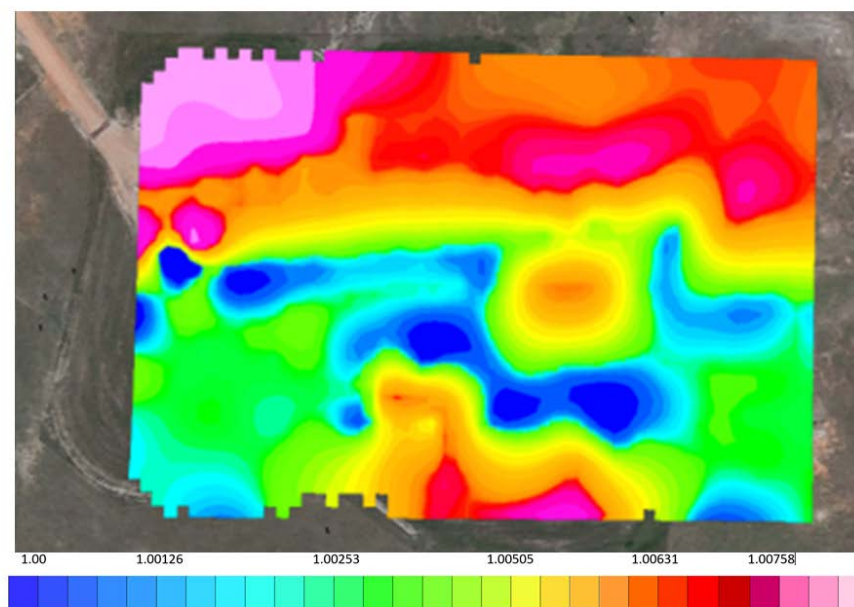
Figure 31: Contour plot of CO$_2$ relative concentrations from trial #4

Both maps suggest that gas concentrations were higher north to the well site. The reason that the concentration was higher at north might be related to traffic on the highway north of the well site. The emission from vehicles could result in higher CH$_4$ and CO$_2$ concentrations. Since the gas flare was shut off, the concentration of targeted gas around the gas flare did not experience any significant changes.

Overall, the field trials demonstrated the effectiveness of this UAV-based air monitoring system. The system successfully measured the air quality over the oil field and provided relatively accurate data. The results were as expected, but weather issues might have affected the data outcomes. Additional field tests are needed in the future.

2.4. Discussion

Although only a limited number of tests were performed in the field, the data feedback is rather impressive. Given that the weather conditions were not optimal for air quality monitoring, the data outcome may have been affected. The first three trials performed at well #1 had the most convincing outcomes, as the data set was relatively large compared to that from the fourth trial performed at well #2. Despite this disadvantage, the fourth trial still showed some definite characteristics of the well site. In short, all results drawn from data analysis showed that gas concentrations were typically higher around the gas flare, which is commonly found in most of the oil fields (Elvidge, et al., 2009). This result proved the sensitivity of the UBAMS system even at lower concentrations. Comparing our result with the study by Eugster and Kling (2012), several similarities were found, mainly because the same CH_4 sensor was used in both projects. In that paper, the authors stated that the low temperature might have caused the sensor's uncertainty behavior. Thus, the monitoring accuracy might be affected at the low temperature encountered during their field test. This might explain a relatively small fluctuation in data outcomes observed during our field test. For scenarios where low temperature was a notable issue, several factors must be taken into consideration for a more accurate result. First, calibration of the sensors at lower temperatures must be done before deployment. Since the UAV is limited to a finite amount of operating time, it is essential to seek the timing when weather allows for a decent performance.

Even though ultra-long-range communications were not considered in this study, the designed UBAMS system showed the capability of covering the entire oil production site. As aforementioned, the UBAMS system was tested with a maximum communication range of 800 m with the existing setup. It is suitable for most applications in an oil field. Similar studies have validated a greater transmission radius with projects equipped with LoRa modulation, in

scenarios where more extended range is desired. One study was done by Aloys et al. suggested that LoRa can offer adequate network coverage of up to 3 km in a suburban area with dense residential dwellings (Augustin, Yi, Clausen, & Townsley, 2016). The study also showed that to achieve the most extended range, data rate must be reduced to compensate for the loss in signal strength. It was not an issue with this project. However, if the pilot needs to stay at one location and multiple sites need to be inspected at once, the data string length must be shortened to secure the communication stability. Also, Carlos A. Trasviña-Moreno suggested that tweaking of LoRa radio frequency can result in an extended range with less data loss (2016). Increasing the spreading factor to 256 chips/symbol, transmissions could be sent to a receiver station at approximately 7 km (Trasviña-Moreno, Blasco, Casas, & Asensio, 2016). Although a smaller bandwidth and a lower coding rate are needed, an estimate of only 3.1 kbps of maximum bitrate can be achieved. Yet this bitrate is still effective enough for this project. In reality, a regular UAV cannot reach 7 km in distance. Thus, this is not considered for this project.

The limitations of the system quickly became apparent during the field tests. The operation and performance of the UAV air monitoring system were highly weather dependent. Under extreme weather conditions with such as snow shower and strong winds, the operation became uncontrollable. At higher altitudes and under load, the UAV's performance decrease as well. Despite the limitations, UAV applications are still a good solution when monitoring air quality in areas with poor accessibility. In a similar project done by Oscar et al., the author states that several aspects need to be addressed, including cooperation, collision avoidance, and communication. Using mobile sensors installed on UAVs also brings up new issues to the monitoring process, including altitude and wind (Alvear, Zema, Natalizio, & Calafate, 2017). Regardless of these aspects, using UAV in air monitoring services is still a good option because

of their flexibility and relatively low cost and their ability to monitor remote areas that are difficult to access.

2.5. Conclusion

A UAV-based air monitoring system (UBAMS) was successfully designed and fabricated for CH_4 and CO_2 monitoring over an oil field. The airborne sensor node was comprised of low-cost gas sensors, an Arduino microcontroller, a GPS module, an SD card shield, and a LoRa wireless transmitter. The ground station consisted of a microcontroller and a LoRa wireless receiver. A graphic user interface (GUI) was created to visualize and record data on a laptop computer. The system was first tested near the university campus, where the preliminary test showed that the airborne sensor was able to measure CH_4 and CO_2 concentrations and send real-time monitoring data to the ground station and then the GUI. The system was further tested at two active oil production sites, and the test results revealed a non-uniform distribution of CH_4 and CO_2 concentrations over the sites due to flare and traffic. Despite issues such as the poor sensitivity of selected gas sensors, the UBAMS has demonstrated its great potential as a simple, low-cost solution to air monitoring tasks, including air quality survey and gas leakage detection, in oil fields. The UBAMS system can also be used for other applications such as forest fire smoke and air quality monitoring in underground mines, upon minor revisions.

Chapter 3

3. Conclusion and Recommendations

3.1. Conclusion

This project aimed to design and fabricate a UAV-based air monitoring system (UBAMS) to monitor air pollutant emissions over an oil field. The main objective of this project is to use off-the-shelf sensors and microcontrollers to build a functional unit that can sense a certain type of pollutants, specifically CO_2 and CH_4. To accomplish this goal, the sensors must be power efficient, low cost, lightweight and effective. Thus, a TGS 2600 sensor was selected to measure CH_4 concentration and an MH-Z14A sensor was selected to measure CO_2 concentrations. These sensors were tested at various conditions and they were proved to meet all criteria listed above. The UBAMS system also includes a microcontroller to process all the information sent in and out, a GPS sensor to measure the location and time, a temperature and humidity sensor to work along with TGS 2600 sensor and an SD card shield to store data. It was determined that the designed system was able to measure pollutants concentration at lower concentration (1.8 ppm of CH_4 and 400 ppm of CO_2, respectively) as well as higher concentration scenarios. The UBAMS system could record and send out a 70-byte data string every 2 seconds; this enabled the possibility of using software to model the gas concentration over an entire oil field. One aspect worth mentioning is the system cost only around 300 dollars and weighs less than 600 grams, which achieved the low cost and lightweight objectives.

When considering building a wireless solution to achieve a "real-time" data transmission, the Long-Range wireless protocol (LoRa) served the purpose well. It was able to successfully send a 70-byte data string to the ground station every 2 seconds in a stable manner. It was a low power consumption unit, and this ensured the overall stability of the entire system. With the

current settings (13 dBm output power, 915.0 MHz of frequency, 62,500 bit/s of bandwidth, and a spreading factor of 9), the unit was able to achieve a 800-m communication range. Although longer range can be achieved by changing the setups, it is not necessary or recommended for this project. Also, a graphic user interface (GUI) was created to work alongside with LoRa by using NI LabVIEW. This provided an intuitive view of the real-time sensing data and enabled auto-logging in a personal PC.

The system was tested near the university campus and at two active oil production sites. The latter represents a more challenging yet real working environment. The Oasis Montaj was used for modeling and mapping aspects. The limitations of the system became apparent during the field test and the post-field test analysis. First, the system is weather dependent, during the field test, low temperature and light precipitation was observed (15 °F and 50-80% RH respectively), the performance of the UAV was decreased significantly. Second, an 8-mph wind speed was detected during the test, this not only decreased the performance of the UAV but also increased the air diffusion on a large scale. At higher altitudes (45 m), the air diffusion became more significant; this was shown with the Oasis Montaj model. The model also states that the pollutant concentration is always higher around the gas flare, which make sense in real-world situations. Furthermore, although limitations apply, the UBAMS system achieved all the objectives of this project.

3.2. Recommendations

In order to achieve the best performance in the future, sensor calibration is needed. This study did not have the opportunity to calibrate any of the sensors, but that would be a necessary next step.

Also, more field test should be performed in the future. The field tests should not be limited to the oil fields, but also other methane-rich environments such as wetlands. This would give a comprehensive review of how the system performance in different environments.

Finally, any personal plans to perform such tasks should be aware of the limitations of the system. Fly overload and severe weather conditions can cause many unexpected accidents. Fly at better conditions can also speed up the data collection process as well as improve the data accuracy.

4. References

Al-Haija, Q. A., Al-Qadeeb, H., & Al-Lwaimi, A. (2013). Case Study: Monitoring of AIR
quality in King Faisal University using a microcontroller and WSN. *Procedia Computer
Science, 21*, 517 – 521.

Alvarez, R. A., Pacala, S. W., Winebrake, J. J., Chameides, W. L., & Hamburg, S. P. (2012).
Greater focus needed on methane leakage from natural gas infrastructure. *PNAS*, 6435-
6440.

Alvear, O., Zema, N. R., Natalizio, E., & Calafate, C. T. (2017). Using UAV-Based Systems to
Monitor Air Pollution in Areas with Poor Accessibility. *Journal of Advanced
Transportation*, 1-14.

Arduino Mega. (2018, November 13). Retrieved from Arduino:
https://www.arduino.cc/en/Main/arduinoBoardMega/

Arduino Mega. (2018, November 13). Retrieved from Mantech:
http://www.mantech.co.za/datasheets/products/A000047.pdf

Augustin, A., Yi, J., Clausen, T., & Townsley, W. M. (2016). A Study of LoRa: Long Range &
Low Power Networks for the Internet of Things. (D. Kim, Ed.) *Sensors*, 1-18.

B_E_N. (2018, November 13). *What is an Arduino?* Retrieved from Sparkfun:
https://learn.sparkfun.com/tutorials/what-is-an-arduino

Capteur Sensors. (2000). General Information on the Capteur NGL07 Carbon Monoxide Sensors.
In *Capteur Sensors* (pp. 1-13). U.K.

Centenaro, M., Vangelista, L., Zanella, A., & Zorzi, M. (2016). Long-Range Communications in
Unlicensed Bands:. *IEEE Wireless Communications*, 2-8.

Elvidge, C. D., Ziskin, D., Baugh, K. E., Tuttle, B. T., Ghosh, T., Pack, D. W., Erwin, E.H.,
Zhizhin, M. (2009, August 7). A Fifteen Year Record of Global Natural Gas Flaring
Derived from Satellite Data. *Energies*, pp. 595-622.

Eugster, W., & Kling, G. W. (2012). Performance of a low-cost methane sensor for ambient.
Atmospheric Measurement Techniques, 1-10.

Hashmonay, R. A., & Ramsey, S. H. (2018, April 25). *Long-Term, Open-Path Emissions
Monitoring at Oil and Gas.* Retrieved from USEPA:
https://www3.epa.gov/ttnchie1/conference/ei20/session7/rhashmonay.pdf

Howarth, R. W., Santoro, R., & Ingraffea, A. (2011). Methane and the greenhouse-gas footprint
of natural gas from shale formations. *Climate Change*, 679-690.

Intergovernmental Panel on Climate Change. (2007). *Climate Change 2007: The Physical
Science Basis.* Cambridge Univ. Press, New York: Contribution of Working Group I to
the Fourth Assessment Report of the Intergovernmental Panel on Climate Change.

International Civil Aviation Organization. (2016). *Unmanned Aircraft Systems (UAS).* Montréal,
Quebec, Canada: ICAO.

Khan, A., Schaefer, D., Lei Tao, D. J., Sun, K., Zondlo, M. A., Harrison, W. A., Roscoe, B.,
Lary, D. J. (2012). Low Power Greenhouse Gas Sensors for Unmanned Aerial Vehicles .
Remote Sensing , 1355-1368.

Kirchgessner, D. A., Lott, R. A., Cowgill, R. M., Harrison, M. R., & Shires, T. M. (1999).
Estimate of Methane Emissions from the U.S. Natural Gas Industry. Research Triangle
Park: U.S. Environmental Protection Agency Air Pollution Prevention and Control
Division.

Kularatna, N., & Sudantha, B. (2008, April). An Environmental Air Pollution Monitoring
System Based on the IEEE 1451 Standard for Low Cost Requirements. *IEEE Sensors
Journal, 8*(4), 415-422.

Macey, G. P., Breech, R., Chernaik, M., Cox , C., Larsen, D., Thomas, D., & Carpenter, D. O.
(2014). Air concentrations of volatile compounds near oil and gas production: a
community-based exploratory study. *Environmental Health*, 13(82), 1-18.

Overview of the Petroleum Geology of the North Dakota Williston Basin. (2018, November 14).
Retrieved from North Dakota Geological Survey:
https://www.dmr.nd.gov/ndgs/resources/

Shrivastava, A., Prabhaker, R., Kumar, R., & Verma, R. (2013). GSM Based Gas Leakage
Detection System. *International Journal of Technical Research and Applications*, 42-45.

Trasviña-Moreno, C. A., Blasco, R., Casas, R., & Asensio, Á. (2016). A Network Performance
Analysis of LoRa Modulation for LPWAN Sensor Devices. In *Ubiquitous Computing
and Ambient Intelligence,*. Eds. Garcia, C.R., Caballero-Gil, P., Burmester, M., Quesada-
Arencibia, A., pp. 174-181.

U.S. Department of Energy Energy Information Administration. (1999). *Natural Gas 1998:
Issues and Trends.* U.S. Department of Energy Energy Information Administration.

U.S. Energy Information Administration. (2011). *Voluntary Reporting of Greenhouse Gases
Program, Table of Carbon Dioxide Emission*. Retrieved from U.S. Energy Information
Administration: https://www.eia.gov/oiaf/1605/coefficients.html

U.S. Energy Information Administration. (2012). *Shale oil maps. Bakken Shale Play, Williston
Basin, North Dakota, Montana,*. Retrieved from U.S. Energy Information
Administration: https://www.eia.gov/oil&uscore;gas/rpd/shaleoil1.pdf

Walton, J. (2015, October 5). *The US States That Produce the Most Oil*. Retrieved from

    Investopedia: https://www.investopedia.com/articles/investing/100515/us-states-produce-

    most-oil.asp

Watts, A. C., Ambrosia, V. G., & Hinkley, E. A. (2012). Unmanned Aircraft Systems in Remote

    Sensing and Scientific Research: Classification and Considerations of Use. *Remote*

    Sensing, 1671-1692.

Yan, L., Gou, Z., & Duan, Y. (2009). A UAV remote sensing system: Design and Tests.

    Geospatial Technology for Earth Observation, 27-44.

5. Appendix A: Arduino codes

5.1. Code for the UAV Sensor Node

```
#include <SPI.h>
#include <SD.h>
#include <TinyGPS++.h>
#include <cactus_io_DHT22.h>
#include <RH_RF95.h>

/*
  for SD card
  SD card attached to SPI bus as follows:
  MOSI - pin 51
  MISO - pin 50
  CLK - pin 52
  CS - pin 53
*/

// Define a dht object using the DHT22 (temperature & humidity) library
#define DHT22_PIN 33
DHT22 dht(DHT22_PIN);

// 0 refers to SD not working; 1 refers to working
int sdstatus = 0;

// Define a Lora object using the Lora library
RH_RF95 rf95;
// Specify the Lora frequency for North America
float frequency = 915.0;

// Define CS pins for SD card and Lora module; note: for Arduino Mega board
const int SDPin = 53;
const int LoRaPin = 10;

// The TinyGPS++ object
TinyGPSPlus gps;

// Set up variables for methane sensor; note: using analog input at A8
int gasSensor = A8;
int val = 0;

float voMeasured = 0;
float Rs = 0;
float Ratio = 0;
float Ratio_corr = 0;
```

```
      float CH4 = 0;

      // Set up variables for NDIR CO2 sensor
      const byte requestReading[] = {0xFF, 0x01, 0x86, 0x00, 0x00, 0x00, 0x00, 0x00, 0x79};
      byte result[9];


      void setup() {
      // Set the CS pins for SD and Lora as output, thereby allowing for a switch between the
two SPI devices
        pinMode (SDPin, OUTPUT);
        pinMode (LoRaPin, OUTPUT);

        // serial for serial monitor
        Serial.begin(9600);
        // serial2 for CO2
        Serial2.begin(9600);
        // serial3 for GPS
        Serial3.begin(9600);

        // Initialization of DHT sensor reading
        //dht.begin();

        // Disable Lora while enable SD on SPI and then initialize SD card communication
        digitalWrite (LoRaPin, HIGH);
        digitalWrite (SDPin, LOW);

        Serial.print("Initializing SD card...");

        if (!SD.begin(SDPin)) {
          Serial.println("initialization failed!");
          sdstatus = 0;
          return;
        }
        Serial.println("initialization done.");

          // Disable SD while enable LoRa on SPI and then initilize Lora communication
        digitalWrite (SDPin, HIGH);
        digitalWrite (LoRaPin, LOW);
        Serial.print("Start LoRa Client...");
        if (!rf95.init()) {
        Serial.println("initilization failed!");
        return;
        }
        Serial.println("initialization done.");
        // Setup ISM frequency
```

```
        rf95.setFrequency(frequency);
        // Setup Power,dBm
        rf95.setTxPower(13);
        // Setup Spreading Factor (6 ~ 12)
        rf95.setSpreadingFactor(9);
        // Setup BandWidth, option:
7800,10400,15600,20800,31200,41700,62500,125000,250000,500000
        // Lower BandWidth for longer distance.
        rf95.setSignalBandwidth(62500);
        // Setup Coding Rate:5(4/5),6(4/6),7(4/7),8(4/8)
        rf95.setCodingRate4(6);
      }

      void loop() {
        // Set up a string to save the data
        String dataString = "";

        // Read GPS signals every 2 seconds
        unsigned long start = millis();
        do
        {
          while (Serial3.available())
            gps.encode(Serial3.read());
        } while (millis() - start < 1000);
      //{

        if (gps.time.isValid()) // Read time info from the GPS module
        {
          dataString = String(gps.time.value()) + ",";
        }
        else
        {
          dataString = "-999,"; // Note: assign invalid GPS signals as -999 for diagnostic purpose
          Serial.print(F("GPS TIME INVALID"));
        }

        if (gps.location.isValid()) // Read lat, long, and elevation info from the GPS module
        {
          dataString = dataString + String(gps.location.lat(),6) + "," +
String(gps.location.lng(),6) + "," + String(gps.altitude.meters()) + ",";
        }
        else // If not sucessful, display the current number of satellites available; note: at least 4
satellites are needed.
        {
          dataString = dataString + "-999,-999,-999,"; // Note: assign invalid GPS signals as -
999 for diagnostic purpose
```

```
       Serial.print(F("GPS LOCATION INVALID"));
       Serial.print(F(" # of satellites available: "));
       Serial.println(gps.satellites.value());
      }

       // Read temperature and humidity readings and store them to variables hum and temp
      dht.readHumidity();
      dht.readTemperature();

     if (isnan(dht.humidity) || isnan(dht.temperature_C)) {
       //Serial.print("Read DHT22 failed");
       return;
      }

      // Read CH4 concentration from analog input A8 and correct it with humidity and
temperature data
       voMeasured = analogRead(gasSensor); // read the value from the port A8
       voMeasured = voMeasured/1023*5.0; // note: analogRead translate 0-5 V to 0-1023
       Rs = (5.0 * 2.5)/voMeasured - 2.5;
       Ratio = Rs/200;  // question: why R0 = -2.1875 kohm?
       Ratio_corr=Ratio*(0.024+0.072*dht.humidity+0.0246*dht.temperature_C);// note:
Rs/R0 should be multiplied by the T&RH correction factor
       Serial.print(F("Rs/R0 = "));
       Serial.println(Ratio_corr);
        CH4=1.8 + 0.1/Ratio_corr; // note: based on the sensor manual, we should use '/' not '*'

       dataString = dataString + String(CH4)+ ",";

       // Read CO2 concentration from the CO2 sensor via digital pin 33
       int ppmS = readPPMSerial();
       dataString = dataString + String(ppmS)+ "," ;

       dataString = dataString + String(dht.temperature_C)+ "," + String(dht.humidity) +  "," +
String(sdstatus) + " ";

      // }

      // Disable SD but enable LoRa on SPI
      digitalWrite (SDPin, HIGH);
      digitalWrite (LoRaPin, LOW);


      // Send a message to LoRa Server
      unsigned int StrLen = dataString.length();
      byte data[StrLen];
      dataString.toCharArray(data, StrLen);
```

```
          rf95.send(data, sizeof(data));

          delay(500);

          if (gps.date.isValid()) // Read date info from the GPS module
          {
           dataString = String(gps.date.value()) + "," + dataString;
          }
          else
          {
           dataString = "-999," + dataString; // Note: assign invalid GPS signals as -999 for
diagnostic purpose
           Serial.print(F("GPS DATE INVALID"));
          }

          //disable LoRa but enable SD on SPI
          digitalWrite (LoRaPin, HIGH);
          digitalWrite (SDPin, LOW);

          File dataFile = SD.open("data.txt", FILE_WRITE);
          // if the file is available, write to it:
          if (dataFile) {
           //Serial.println("Save to SD card");
           dataFile.println(dataString);
           dataFile.close();
           sdstatus = 1;
           // print to the serial port too:
          Serial.println(dataString);
          }
          // if the file isn't open, pop up an error:
          else {
           Serial.println("error opening data.txt");
           sdstatus = 0;
           Serial.println(dataString);
          }

         long programend = millis() - start;
         programend = 2000 - programend;
         if (programend < 0)
         {
          programend = 0;
         }
         else
         {
           ;
           }
```

```
  delay(programend);
}


int readPPMSerial() {
  for (int i = 0; i < 9; i++) {
    Serial2.write(requestReading[i]);
  }
  while (Serial2.available() < 9) {}; // wait for response
  for (int i = 0; i < 9; i++) {
    result[i] = Serial2.read();
  }
  int high = result[2];
  int low = result[3];
    //Serial.print(high); Serial.print(" ");Serial.println(low);
  return high * 256 + low;
}
```

5.2. Code for the Ground Station

```
#include <SPI.h>
#include <RH_RF95.h>

// Singleton instance of the radio driver
RH_RF95 rf95;

//int led = A2;
float frequency = 915.0;

void setup()
{
 //pinMode(led, OUTPUT);
 Serial.begin(9600);
 while (!Serial) ; // Wait for serial port to be available
 Serial.println("Lora init");
 if (!rf95.init())
   Serial.println("init failed");
 // Setup ISM frequency
 rf95.setFrequency(frequency);
 // Setup Power,dBm
 rf95.setTxPower(13);
 // Setup Spreading Factor (6 ~ 12)
 rf95.setSpreadingFactor(9);
 // Setup BandWidth, option: 7800, 10400, 15600, 20800, 31200, 41700, 62500, 125000,
250000, 500000
 // Lower BandWidth for longer distance.
 rf95.setSignalBandwidth(62500);
 // Setup Coding Rate:5(4/5),6(4/6),7(4/7),8(4/8)
 rf95.setCodingRate4(6);
}

void loop()
{
 if (rf95.available())
 {
  // Should be a message for us now
  uint8_t buf[RH_RF95_MAX_MESSAGE_LEN];
  uint8_t len = sizeof(buf);
  if (rf95.recv(buf, &len))
  {
   Serial.print((char*)buf);
   Serial.print(",");
   Serial.print(len, DEC);
   Serial.print(",");
   Serial.println(rf95.lastRssi(), DEC);
```

```
      }
    else
    {
      Serial.println("recv failed");
    }
  }
}
```

6. Appendix B: Data Obtained from Field Tests

Table I: Field test data at well #1 – Trial #1

time	latitude	longitude	elevation	Methane conc. (ppm)	CO₂ conc. (ppm)
18421200	47.67231	-103.64124	705.8	1.91	398
18421400	47.67231	-103.64124	705.6	1.89	398
18421600	47.67231	-103.64123	706.2	1.89	398
18421800	47.67231	-103.64123	706.3	1.89	398
18422000	47.67231	-103.64122	705.9	1.88	398
18422200	47.67231	-103.64123	706.8	1.88	398
18422400	47.67231	-103.64123	707.9	1.88	398
18422600	47.67231	-103.64117	707.3	1.88	398
18422800	47.6723	-103.64108	706.6	1.88	398
18423000	47.6723	-103.64102	706.7	1.88	398
18423200	47.6723	-103.64098	706.2	1.88	398
18423400	47.67231	-103.64089	706.1	1.88	398
18423600	47.67232	-103.64077	705.6	1.86	398
18423800	47.67234	-103.64063	705.2	1.86	398
18424000	47.67236	-103.6405	705.4	1.86	398
18424200	47.67235	-103.64045	705.3	1.88	398
18424400	47.6723	-103.64037	705.7	1.88	398
18424600	47.67223	-103.64029	705.3	1.88	398
18424800	47.67215	-103.64024	705.5	1.89	398
18425000	47.67213	-103.64023	705.6	1.88	398
18425200	47.67213	-103.64019	705.5	1.89	398
18425400	47.67213	-103.64011	705.6	1.89	398
18425600	47.67218	-103.64002	709.7	1.88	398
18425800	47.67225	-103.63998	709.5	1.88	398
18430000	47.67225	-103.63999	708.1	1.87	398
18430200	47.67222	-103.64003	709	1.88	398
18430400	47.67218	-103.64005	710.2	1.87	398
18430600	47.67218	-103.64003	716.9	1.88	398
18430800	47.67218	-103.64004	717.7	1.87	398
18431000	47.67216	-103.64008	718.7	1.88	398
18431200	47.67213	-103.64017	719.8	1.87	398
18431400	47.67211	-103.64027	722.2	1.88	398
18431600	47.67209	-103.64043	723	1.87	397
18431800	47.67207	-103.64061	724.4	1.87	397
18432000	47.67208	-103.64082	725.6	1.87	397
18432200	47.67209	-103.64108	725.7	1.88	397

18432400	47.6721	-103.64137	726	1.87	397
18432600	47.6721	-103.64166	725.9	1.86	397
18432800	47.6721	-103.64183	727.2	1.85	397
18433000	47.6721	-103.64183	727.6	1.87	397
18433200	47.67215	-103.64185	728.5	1.87	397
18433400	47.67221	-103.64186	728.8	1.87	397
18433600	47.6722	-103.64186	728.3	1.87	397
18433800	47.67221	-103.6418	727.4	1.87	397
18434000	47.67222	-103.64169	726.5	1.86	397
18434200	47.67223	-103.64157	725.4	1.84	398
18434400	47.67226	-103.64143	724.8	1.85	398
18434600	47.67228	-103.64128	723.8	1.84	398
18434800	47.67229	-103.64108	723.7	1.85	398
18435000	47.6723	-103.64086	724.5	1.87	398
18435200	47.6723	-103.64063	725.5	1.86	398
18435400	47.67229	-103.6404	725.8	1.86	398
18435600	47.67229	-103.64017	725.9	1.87	398
18435800	47.67228	-103.63995	726.4	1.87	398
18440000	47.67227	-103.63973	725.7	1.87	398
18440200	47.67225	-103.63958	725.8	1.86	398
18440400	47.67224	-103.63957	726.9	1.86	398
18440600	47.67233	-103.63961	727.5	1.85	398
18440800	47.67241	-103.63965	727.9	1.87	398
18441000	47.67241	-103.63965	726.9	1.86	398
18441200	47.67238	-103.63972	726.6	1.87	398
18441400	47.67236	-103.63985	727.3	1.88	398
18441600	47.67234	-103.64002	727.3	1.86	398
18441800	47.67233	-103.64021	727.3	1.87	398
18442000	47.67233	-103.64043	727.3	1.87	398
18442200	47.67232	-103.64066	727.1	1.87	398
18442400	47.6723	-103.64091	727.4	1.86	398
18442600	47.67226	-103.64117	728.1	1.86	397
18442800	47.67223	-103.64144	728.7	1.86	397
18443000	47.67218	-103.64167	728.9	1.85	397
18443200	47.67217	-103.64167	727.8	1.85	397
18443400	47.67222	-103.64165	725.6	1.85	397
18443600	47.67231	-103.64165	725.3	1.86	397
18443800	47.67231	-103.64164	726.1	1.86	397
18444000	47.67231	-103.64153	724.9	1.87	397
18444200	47.67232	-103.64138	723.9	1.86	397
18444400	47.67234	-103.64121	723	1.86	397

18444600	47.67237	-103.64101	723.6	1.87	397
18444800	47.67242	-103.64081	723.8	1.86	397
18445000	47.67244	-103.64066	724.5	1.86	397
18445200	47.67242	-103.6405	725.2	1.85	397
18445400	47.67241	-103.64047	724.2	1.86	397
18445600	47.67241	-103.64047	724.8	1.85	397
18445800	47.6724	-103.64043	725.6	1.85	397
18450000	47.67238	-103.6403	726.3	1.85	397
18450200	47.67236	-103.64014	726.3	1.85	397
18450400	47.67236	-103.63997	726.7	1.85	397
18450600	47.67236	-103.63976	726.8	1.86	397
18450800	47.67236	-103.63958	726.5	1.85	397
18451000	47.67237	-103.63953	727	1.85	397
18451200	47.67245	-103.63946	727.5	1.85	397
18451400	47.67247	-103.63943	728	1.86	397
18451600	47.67246	-103.63945	728.4	1.84	397
18451800	47.67247	-103.63953	729.6	1.86	397
18452000	47.67249	-103.63966	729.3	1.85	397
18452200	47.67248	-103.63984	729.1	1.86	397
18452400	47.67247	-103.64004	729	1.85	397
18452600	47.67247	-103.64027	729	1.85	397
18452800	47.67246	-103.64053	728.8	1.85	397
18453000	47.67244	-103.64082	729.4	1.84	397
18453200	47.6724	-103.64111	729.6	1.84	397
18453400	47.67234	-103.6414	729.1	1.84	397
18453600	47.67227	-103.64164	728.7	1.84	397
18453800	47.67222	-103.64181	731	1.84	397
18454000	47.67223	-103.64178	730.9	1.85	397
18454200	47.67234	-103.64172	732	1.85	397
18454400	47.67249	-103.64166	731.6	1.85	397
18454600	47.67252	-103.64165	729.6	1.85	397
18454800	47.67249	-103.64154	727.5	1.85	397
18455000	47.67248	-103.64137	726.6	1.84	397
18455200	47.67248	-103.64115	726.5	1.85	397
18455400	47.67249	-103.6409	725.9	1.85	397
18455600	47.6725	-103.64063	725.1	1.85	397
18455800	47.67252	-103.64035	725	1.85	397
18460000	47.67255	-103.64009	725.7	1.84	397
18460200	47.67259	-103.63986	725.7	1.85	397
18460400	47.67262	-103.6397	726.3	1.84	397
18460600	47.67264	-103.63955	726.3	1.84	397

18460800	47.67266	-103.63944	727.2	1.85	397
18461000	47.67269	-103.63939	729	1.85	397
18461200	47.67278	-103.63931	730.3	1.85	397
18461400	47.67278	-103.6393	731.6	1.85	397
18461600	47.67279	-103.63928	731.3	1.84	397
18461800	47.67284	-103.63927	730.5	1.84	397
18462000	47.67288	-103.6393	730.8	1.85	397
18462200	47.67288	-103.63938	730.1	1.84	397
18462400	47.67283	-103.63947	729.3	1.86	397
18462600	47.6728	-103.63959	731.7	1.84	397
18462800	47.67278	-103.63973	731.9	1.83	397
18463000	47.67276	-103.63991	732.1	1.85	397
18463200	47.67273	-103.64011	731.3	1.84	397
18463400	47.67271	-103.6403	731.3	1.84	397
18463600	47.67269	-103.6405	731.2	1.85	397
18463800	47.67266	-103.64071	731.4	1.85	397
18464000	47.67264	-103.64093	731.5	1.84	397
18464200	47.67265	-103.64114	731.9	1.84	397
18464400	47.67266	-103.64137	731.5	1.86	397
18464600	47.67263	-103.64161	730.6	1.84	397
18464800	47.67261	-103.64181	730.8	1.84	397
18465000	47.6726	-103.64182	730	1.83	397
18465200	47.67266	-103.64175	729.4	1.84	397
18465400	47.67277	-103.64167	729.2	1.84	397
18465600	47.6728	-103.64163	729.5	1.83	398
18465800	47.67279	-103.64148	727.9	1.85	398
18470000	47.67278	-103.64128	728.1	1.84	398
18470200	47.67279	-103.64106	728.4	1.84	398
18470400	47.67281	-103.64083	727.5	1.84	398
18470600	47.67283	-103.64059	727.9	1.84	398
18470800	47.67282	-103.64036	727.8	1.84	398
18471000	47.6728	-103.64026	728.2	1.85	398
18471200	47.6728	-103.64011	728.7	1.84	398
18471400	47.67281	-103.63986	729.2	1.84	398
18471600	47.67284	-103.63961	729.7	1.85	398
18471800	47.67285	-103.63949	728.9	1.84	398
18472000	47.67294	-103.63942	729.6	1.84	398
18472200	47.67308	-103.63934	730.3	1.84	398
18472400	47.6731	-103.63934	730.7	1.84	398
18472600	47.67315	-103.63942	731.2	1.84	398
18472800	47.67322	-103.63959	730	1.85	398

18473000	47.67325	-103.63982	728.7	1.85	398
18473200	47.67322	-103.64007	729.1	1.84	398
18473400	47.67325	-103.64028	730.9	1.84	398
18473600	47.67332	-103.6405	731.3	1.84	398
18473800	47.67337	-103.64075	730.4	1.84	398
18474000	47.67338	-103.64101	731.1	1.83	398
18474200	47.67338	-103.64129	731.6	1.84	398
18474400	47.67337	-103.64158	732.2	1.84	398
18474600	47.67335	-103.64186	732	1.84	398
18474800	47.67332	-103.64211	732.1	1.84	398
18475000	47.67329	-103.64216	732.1	1.84	398
18475200	47.6732	-103.64211	731.3	1.84	398
18475400	47.67309	-103.64199	730.4	1.85	398
18475600	47.67299	-103.64185	729.9	1.85	398
18475800	47.67289	-103.64172	730.8	1.85	398
18480000	47.67277	-103.64167	731.3	1.84	398
18480200	47.6727	-103.64165	731	1.84	398
18480400	47.67263	-103.64164	730.9	1.84	398
18480600	47.67253	-103.64164	731.1	1.84	398
18480800	47.67244	-103.64159	731	1.84	398
18481000	47.67237	-103.64153	732.1	1.84	398
18481200	47.67232	-103.64146	732.5	1.84	398
18481400	47.6723	-103.64144	733.7	1.85	398
18481600	47.67226	-103.6414	734.7	1.84	398
18481800	47.67226	-103.6414	732.7	1.83	398
18482000	47.67226	-103.6414	729.6	1.83	398
18482200	47.67226	-103.64136	726.3	1.85	398
18482400	47.67226	-103.64129	723.2	1.84	398
18482600	47.67226	-103.64127	717.7	1.85	398
18482800	47.67227	-103.64127	713.2	1.83	398
18483000	47.67228	-103.64127	708.8	1.84	398
18483200	47.67228	-103.64126	707.4	1.84	398
18483400	47.67228	-103.64124	707.3	1.84	398
18483600	47.67232	-103.6412	707.5	1.84	398
18483800	47.67233	-103.6412	706.1	1.83	398
18484000	47.67233	-103.6412	705.5	1.84	398
18484200	47.67233	-103.6412	704.2	1.84	398
18484400	47.67233	-103.64119	703.4	1.84	398
18484600	47.67234	-103.64118	703.1	1.84	398
18484800	47.67234	-103.64118	702.9	1.84	398
18485000	47.67235	-103.64118	702.2	1.84	398

18485200	47.67236	-103.64117	702	1.84	398
18485400	47.67237	-103.64117	701.6	1.84	398
18485700	47.67236	-103.64117	702.1	1.84	398
18485900	47.67237	-103.64117	701.7	1.85	398
18490100	47.67237	-103.64117	701.2	1.84	398
18490300	47.67237	-103.64117	700.8	1.84	398
18490500	47.67237	-103.64117	700.4	1.84	398
18490700	47.67237	-103.64117	700.3	1.84	398
18490900	47.67237	-103.64116	699.7	1.84	398
18491100	47.67237	-103.64116	699.1	1.84	398
18491300	47.67238	-103.64116	698.9	1.84	398
18491500	47.67238	-103.64116	698.3	1.85	398
18491700	47.67238	-103.64116	698.3	1.84	398
18491900	47.67238	-103.64116	698.3	1.84	398
18492100	47.67238	-103.64116	698.3	1.85	398
18492300	47.67238	-103.64117	698.3	1.84	398
18492500	47.67238	-103.64117	698	1.85	398
18492700	47.67239	-103.64117	698	1.85	398
18492900	47.67239	-103.64117	698.2	1.84	398

Table II: Field test data at well #1 – Trial #2

latitude	longitude	elevation	Methane conc. (ppm)	CO_2 conc. (ppm)
47.67227	-103.641	712.7	1.84	398
47.67228	-103.641	712.7	1.85	398
47.67222	-103.641	712.7	1.86	398
47.67218	-103.641	712.7	1.86	398
47.67218	-103.641	713.3	1.86	398
47.67218	-103.641	713.6	1.87	398
47.6722	-103.64	713.4	1.87	398
47.67222	-103.64	713.6	1.87	398
47.67223	-103.64	714	1.86	398
47.67223	-103.64	713.4	1.86	398
47.67218	-103.64	713.7	1.86	398
47.67213	-103.64	713.7	1.85	398
47.67213	-103.64	713.5	1.86	398
47.67213	-103.64	713.7	1.87	398
47.67212	-103.64	712.1	1.86	398
47.67215	-103.64	712	1.86	398
47.6722	-103.64	712	1.87	397
47.67228	-103.64	712.1	1.86	397
47.67232	-103.64	712.6	1.85	397
47.67233	-103.64	713	1.86	397
47.67234	-103.64	713.3	1.86	397
47.67234	-103.64	713.2	1.87	397
47.67233	-103.641	712.9	1.86	397
47.67233	-103.641	712.7	1.85	397
47.67232	-103.641	712.8	1.86	397
47.67232	-103.641	712.6	1.85	397
47.67233	-103.641	712	1.86	397
47.67233	-103.641	711.9	1.86	397
47.67234	-103.641	711.3	1.85	397
47.67234	-103.641	710.9	1.84	397
47.67234	-103.641	711	1.85	397
47.67234	-103.641	710.4	1.86	397
47.67234	-103.641	709.7	1.85	397
47.67236	-103.641	709.2	1.84	397
47.67239	-103.641	707.8	1.85	397
47.6724	-103.641	706.9	1.85	397
47.67241	-103.641	705.8	1.86	397
47.67241	-103.641	704.9	1.86	397

47.67241	-103.641	704.2	1.86	397
47.67242	-103.641	703.8	1.86	397
47.67242	-103.641	703.6	1.84	397
47.67244	-103.641	703.6	1.85	397
47.67246	-103.641	703.3	1.84	397
47.67248	-103.641	703	1.86	397
47.6725	-103.641	703.7	1.86	397
47.6725	-103.641	704.6	1.85	397
47.67249	-103.641	705.5	1.86	397
47.67248	-103.641	705.8	1.85	397
47.67246	-103.641	706.7	1.85	397
47.67245	-103.641	707.6	1.85	397
47.67244	-103.641	708	1.85	397
47.67243	-103.64	707.9	1.84	397
47.67242	-103.64	708.1	1.85	397
47.67242	-103.64	707.7	1.85	397
47.67241	-103.64	707.5	1.85	397
47.67241	-103.64	707.6	1.84	397
47.67241	-103.64	708	1.86	397
47.67242	-103.64	708.1	1.85	397
47.67242	-103.64	707.5	1.85	397
47.67241	-103.64	707.8	1.83	397
47.67245	-103.64	707.7	1.85	397
47.67249	-103.64	708	1.84	397
47.6725	-103.64	707.5	1.85	397
47.6725	-103.64	707.9	1.85	397
47.67252	-103.64	708.5	1.85	397
47.67254	-103.64	708.7	1.85	397
47.67256	-103.64	708.8	1.85	397
47.67257	-103.641	708.8	1.85	397
47.67257	-103.641	708.7	1.84	397
47.67256	-103.641	708.7	1.84	397
47.67255	-103.641	708.8	1.85	397
47.67253	-103.641	709	1.85	397
47.67251	-103.641	708.8	1.84	397
47.6725	-103.642	708.7	1.85	397
47.67249	-103.642	708.9	1.85	397
47.67249	-103.642	708.3	1.84	397
47.67249	-103.642	708	1.84	397
47.67252	-103.642	707.5	1.84	397
47.67254	-103.642	707.3	1.84	397

47.67255	-103.642	707.6	1.84	397
47.67256	-103.642	707.7	1.83	397
47.67255	-103.641	707.5	1.84	397
47.67257	-103.641	707.2	1.84	397
47.67259	-103.641	707	1.84	397
47.67263	-103.641	707.1	1.83	397
47.67266	-103.641	707.2	1.84	397
47.67269	-103.641	707	1.83	397
47.6727	-103.641	706.4	1.84	397
47.67269	-103.641	706.4	1.85	397
47.67269	-103.641	706.1	1.85	397
47.67269	-103.641	706.5	1.84	397
47.67268	-103.641	706.2	1.84	397
47.67268	-103.641	706.5	1.84	397
47.67269	-103.641	707.7	1.83	397
47.6727	-103.641	709	1.84	397
47.67271	-103.641	709.6	1.83	397
47.67273	-103.641	710.3	1.83	397
47.67273	-103.64	711.4	1.84	397
47.67275	-103.64	712.1	1.84	397
47.67275	-103.64	712.9	1.84	397
47.67276	-103.64	713	1.84	397
47.67277	-103.64	713.3	1.84	397
47.67276	-103.64	713.8	1.85	397
47.67277	-103.64	714.1	1.84	397
47.67281	-103.64	714	1.84	397
47.67288	-103.64	714.8	1.84	397
47.67294	-103.64	714.7	1.84	397
47.67294	-103.64	714.8	1.84	397
47.67294	-103.64	715.6	1.85	397
47.67295	-103.64	715.4	1.83	397
47.67298	-103.64	715.7	1.85	397
47.673	-103.64	715.6	1.84	397
47.673	-103.64	715.7	1.84	397
47.67299	-103.641	715.7	1.84	397
47.67297	-103.641	715.8	1.84	397
47.67295	-103.641	716.1	1.84	397
47.67292	-103.641	716.6	1.84	397
47.67286	-103.642	717	1.84	397
47.6728	-103.642	716.9	1.84	397
47.67276	-103.642	716.5	1.84	397

47.67275	-103.642	716.7	1.84	397
47.67273	-103.642	716.3	1.83	397
47.67269	-103.642	716.5	1.84	397
47.67268	-103.642	717	1.84	397
47.67268	-103.642	717.1	1.84	397
47.67268	-103.642	717.1	1.84	397
47.67269	-103.642	717.1	1.83	397
47.67271	-103.641	717.1	1.84	397
47.67274	-103.641	717	1.84	397
47.67278	-103.641	717.3	1.83	397
47.67279	-103.641	716.9	1.83	397
47.67281	-103.641	716.7	1.83	397
47.67282	-103.641	716.5	1.84	397
47.67284	-103.641	716.6	1.83	397
47.67284	-103.641	716.7	1.83	397
47.67284	-103.64	716.8	1.84	397
47.67283	-103.64	717.2	1.83	397
47.67283	-103.64	718.2	1.83	397
47.67281	-103.64	718	1.83	397
47.67281	-103.64	717.9	1.84	397
47.6728	-103.64	718.2	1.85	397
47.67278	-103.64	718.6	1.84	397
47.67273	-103.64	718.7	1.85	397
47.67267	-103.64	718.6	1.84	397
47.67259	-103.64	718.2	1.84	397
47.6725	-103.64	718.4	1.84	397
47.67242	-103.64	718.3	1.84	397
47.67233	-103.64	718.6	1.84	397
47.67224	-103.64	718.9	1.84	397
47.67215	-103.64	718.7	1.84	397
47.6721	-103.64	718.6	1.84	397
47.67209	-103.64	717.4	1.84	397
47.6721	-103.64	717.6	1.84	397
47.6721	-103.64	717.3	1.84	397
47.6721	-103.64	716.8	1.84	397
47.67212	-103.64	716.7	1.84	397
47.67212	-103.64	716.9	1.84	397
47.6721	-103.641	716.6	1.83	397
47.67209	-103.641	716.3	1.84	397
47.67205	-103.641	716.6	1.83	397
47.672	-103.641	716.7	1.84	397

47.67195	-103.641	716.6	1.84	397
47.67191	-103.641	715.4	1.84	397
47.67196	-103.641	715.2	1.84	397
47.67204	-103.641	714.9	1.84	397
47.6721	-103.641	714.9	1.84	397
47.67211	-103.641	714.8	1.84	397
47.67212	-103.641	714.2	1.84	397
47.67212	-103.641	713.1	1.83	397
47.67216	-103.641	712.8	1.84	397
47.67218	-103.641	712.4	1.84	397
47.67218	-103.641	712.4	1.84	397
47.67218	-103.641	712.1	1.84	397
47.67218	-103.641	711.1	1.83	397
47.67223	-103.641	710.5	1.84	397
47.67224	-103.641	709.6	1.84	397
47.67224	-103.641	707.9	1.85	397
47.67224	-103.641	706.5	1.83	397
47.67225	-103.641	705.8	1.84	397
47.6723	-103.641	705.3	1.83	397
47.67233	-103.641	704.2	1.83	397
47.67234	-103.641	704	1.84	397
47.67236	-103.641	703.2	1.84	397
47.67235	-103.641	703.4	1.84	397
47.67234	-103.641	703.5	1.84	397
47.67234	-103.641	703.6	1.84	397
47.67234	-103.641	703.3	1.84	397
47.67234	-103.641	702.9	1.84	397
47.67234	-103.641	702.6	1.83	397
47.67234	-103.641	702.7	1.83	397
47.67234	-103.641	702.4	1.83	397
47.67234	-103.641	702.7	1.84	397
47.67234	-103.641	702.7	1.84	397
47.67234	-103.641	702.9	1.85	397
47.67234	-103.641	703.1	1.84	397
47.67234	-103.641	703.2	1.83	397
47.67234	-103.641	702.9	1.83	397
47.67234	-103.641	702.9	1.84	397

Table III: Field test data at well #1 – Trial #3

latitude	longitude	elevation	Methane conc. (ppm)	CO$_2$ conc. (ppm)
47.67234	-103.641	702.7	1.83	397
47.67236	-103.641	702.6	1.84	397
47.67237	-103.641	702.7	1.84	397
47.67237	-103.641	702.6	1.83	397
47.67238	-103.641	702.3	1.84	397
47.67237	-103.641	702.3	1.83	397
47.67237	-103.641	702.3	1.84	397
47.67238	-103.641	702.3	1.84	397
47.67238	-103.641	702.6	1.83	397
47.67238	-103.641	702.9	1.84	397
47.67238	-103.641	703.2	1.84	397
47.67238	-103.641	703.8	1.84	397
47.67238	-103.641	704.3	1.83	397
47.67237	-103.641	704.7	1.84	397
47.67237	-103.641	705.3	1.84	397
47.67236	-103.641	705.7	1.83	397
47.67236	-103.641	706.4	1.84	397
47.67236	-103.641	706.9	1.84	397
47.67236	-103.641	706.9	1.84	397
47.67237	-103.641	707	1.83	397
47.67237	-103.641	707	1.83	397
47.67237	-103.641	707.1	1.84	397
47.67236	-103.641	707.1	1.84	397
47.67236	-103.641	707.1	1.84	397
47.67236	-103.641	707.1	1.84	397
47.67236	-103.641	707.1	1.84	397
47.67236	-103.641	707.1	1.83	397
47.67236	-103.641	706.9	1.84	397
47.67235	-103.641	707.7	1.84	397
47.67235	-103.641	708.6	1.84	397
47.67234	-103.641	708.8	1.83	397
47.67233	-103.641	709	1.84	397
47.67232	-103.641	708	1.83	397
47.67231	-103.641	708.1	1.83	397
47.67232	-103.641	708.4	1.83	397
47.67232	-103.641	709.2	1.83	397
47.67231	-103.641	709	1.84	397

47.67229	-103.641	708.8	1.83	397
47.67223	-103.641	710.8	1.83	397
47.67221	-103.641	711.3	1.84	397
47.6722	-103.641	710.9	1.84	397
47.67218	-103.641	710.7	1.83	397
47.67217	-103.641	710	1.83	397
47.67216	-103.641	709.4	1.83	397
47.67216	-103.641	708.7	1.83	397
47.67216	-103.641	708.4	1.84	397
47.67217	-103.641	707.9	1.84	397
47.67218	-103.641	707.7	1.84	397
47.67218	-103.641	707.8	1.84	397
47.67217	-103.641	707.7	1.83	397
47.67216	-103.641	707.6	1.84	397
47.67214	-103.641	707.6	1.84	397
47.67212	-103.641	707.3	1.83	397
47.6721	-103.641	707.3	1.84	397
47.67209	-103.64	707	1.83	397
47.67208	-103.64	707.5	1.84	397
47.67207	-103.64	707.4	1.84	397
47.67206	-103.64	707.1	1.84	397
47.67205	-103.64	707.1	1.83	397
47.67207	-103.64	707.3	1.84	397
47.67212	-103.64	707.1	1.84	397
47.67213	-103.64	707.1	1.84	397
47.67215	-103.64	706.8	1.82	397
47.67214	-103.64	706.7	1.83	397
47.67213	-103.64	706.7	1.84	397
47.67211	-103.64	706.5	1.84	397
47.67212	-103.64	706	1.84	397
47.67215	-103.64	706.4	1.83	397
47.67222	-103.64	706.8	1.83	397
47.67223	-103.64	706.3	1.84	397
47.6722	-103.641	705.7	1.84	397
47.6722	-103.641	704.9	1.83	397
47.67219	-103.641	704.5	1.84	397
47.67218	-103.64	704.6	1.83	397
47.67218	-103.64	704.5	1.83	397
47.6722	-103.64	704.6	1.83	397
47.67223	-103.64	704.5	1.84	397
47.67224	-103.64	704.4	1.83	397

47.67222	-103.64	704	1.83	397
47.67217	-103.64	704.2	1.83	397
47.67212	-103.64	704.5	1.83	397
47.67208	-103.64	704.5	1.84	397
47.67207	-103.64	704.6	1.84	397
47.6721	-103.64	704.2	1.83	397
47.67216	-103.64	703.8	1.83	397
47.67221	-103.64	703.7	1.84	397
47.67224	-103.64	703.9	1.83	397
47.67226	-103.64	704.1	1.84	397
47.67223	-103.64	704.5	1.84	397
47.67216	-103.64	704.9	1.84	397
47.67209	-103.64	705.5	1.84	397
47.67202	-103.64	705.6	1.84	397
47.67202	-103.64	705.2	1.84	397
47.67208	-103.64	705.1	1.84	397
47.67214	-103.64	704.7	1.84	397
47.67218	-103.64	704.6	1.83	397
47.67223	-103.64	704.6	1.84	397
47.67229	-103.64	704.3	1.84	397
47.67235	-103.64	704.3	1.84	397
47.67233	-103.64	704.3	1.83	397
47.67231	-103.64	704	1.84	397
47.67233	-103.64	704	1.84	397
47.67234	-103.64	703.9	1.84	397
47.67234	-103.64	704	1.83	397
47.67236	-103.64	704.3	1.83	397
47.67236	-103.64	704.4	1.84	397
47.67234	-103.64	704.1	1.84	397
47.67232	-103.641	703.8	1.84	397
47.67233	-103.641	703.7	1.84	397
47.67235	-103.641	703.4	1.84	397
47.67234	-103.641	703.4	1.83	397
47.67234	-103.641	703.7	1.84	397
47.67233	-103.641	704	1.83	397
47.67233	-103.641	704.1	1.83	397
47.67233	-103.641	704.7	1.84	397
47.67233	-103.641	705	1.84	397
47.67234	-103.641	705.3	1.83	397
47.67234	-103.641	705.4	1.83	397
47.67235	-103.641	705.2	1.83	397

47.67236	-103.641	704.6	1.83	397
47.67235	-103.641	703.9	1.84	397
47.67235	-103.641	703.9	1.83	397
47.67235	-103.641	703.8	1.84	397
47.67235	-103.641	703.5	1.84	397
47.67235	-103.641	703.3	1.84	397
47.67235	-103.641	703.6	1.83	397
47.67235	-103.641	703.4	1.83	397
47.67235	-103.641	703.4	1.83	397
47.67235	-103.641	703.3	1.84	397
47.67234	-103.641	703.4	1.84	397
47.67234	-103.641	703.3	1.83	397
47.67234	-103.641	703	1.83	397
47.67234	-103.641	702.9	1.83	397
47.67233	-103.641	702.3	1.83	397
47.67233	-103.641	701.6	1.84	397
47.67233	-103.641	701	1.83	397
47.67233	-103.641	700.6	1.84	397
47.67233	-103.641	700.4	1.84	397
47.67233	-103.641	700.1	1.83	397
47.67233	-103.641	699.8	1.83	397
47.67233	-103.641	699.8	1.83	397
47.67233	-103.641	699.6	1.83	397
47.67233	-103.641	699.8	1.84	397
47.67233	-103.641	699.5	1.83	397
47.67233	-103.641	699.2	1.84	397
47.67233	-103.641	699	1.84	397
47.67233	-103.641	699	1.84	397
47.67233	-103.641	698.9	1.83	397
47.67233	-103.641	698.9	1.84	397
47.67233	-103.641	698.9	1.83	397
47.67233	-103.641	698.7	1.83	397
47.67233	-103.641	698.9	1.84	397
47.67233	-103.641	698.8	1.83	397
47.67233	-103.641	698.5	1.83	397
47.67233	-103.641	698.3	1.83	397
47.67233	-103.641	698.4	1.83	397
47.67233	-103.641	698.5	1.83	397
47.67233	-103.641	698.5	1.84	397
47.67233	-103.641	698.4	1.84	397
47.67233	-103.641	697.9	1.83	397

47.67233	-103.641	698.1	1.83	397
47.67233	-103.641	697.8	1.84	397
47.67233	-103.641	697.3	1.83	397
47.67233	-103.641	697.4	1.84	397
47.67233	-103.641	697	1.84	397
47.67233	-103.641	696.8	1.84	397
47.67233	-103.641	696.8	1.84	397
47.67233	-103.641	697.3	1.83	397
47.67233	-103.641	697.5	1.83	397
47.67234	-103.641	698	1.83	397
47.67234	-103.641	698.1	1.84	397
47.67234	-103.641	698.1	1.83	397
47.67234	-103.641	698.5	1.83	397
47.67235	-103.641	698.7	1.84	397
47.67235	-103.641	699	1.84	397
47.67235	-103.641	698.6	1.84	397
47.67235	-103.641	698.9	1.84	397
47.67235	-103.641	698.4	1.83	397
47.67235	-103.641	698.6	1.84	397
47.67235	-103.641	698.6	1.84	397
47.67235	-103.641	698.8	1.84	397
47.67235	-103.641	698.6	1.83	397
47.67235	-103.641	698.8	1.84	397
47.67235	-103.641	698.7	1.83	397
47.67235	-103.641	698.3	1.84	397
47.67235	-103.641	698	1.83	397
47.67235	-103.641	698	1.83	397
47.67235	-103.641	697.7	1.84	397
47.67235	-103.641	697.3	1.84	397
47.67235	-103.641	697.5	1.84	397
47.67235	-103.641	697.9	1.84	397
47.67235	-103.641	698.2	1.83	397
47.67236	-103.641	698.6	1.83	397
47.67236	-103.641	699.3	1.84	397
47.67236	-103.641	699.8	1.84	397
47.67236	-103.641	700.5	1.84	397
47.67236	-103.641	700.8	1.84	397
47.67236	-103.641	701.2	1.84	397
47.67236	-103.641	701.4	1.84	397
47.67236	-103.641	701.7	1.84	397
47.67237	-103.641	702	1.84	397

47.67237	-103.641	702.2	1.84	397
47.67237	-103.641	702.4	1.84	397
47.67237	-103.641	702.6	1.84	397
47.67237	-103.641	704.7	1.84	397
47.67236	-103.641	706.2	1.85	397
47.67236	-103.641	706.6	1.86	397
47.67236	-103.641	706.4	1.85	397
47.67235	-103.641	706.2	1.85	397
47.67235	-103.641	704.9	1.85	397
47.67234	-103.641	703.3	1.85	397
47.67233	-103.641	702.6	1.85	397
47.67233	-103.641	701.9	1.84	397
47.67233	-103.641	702.1	1.84	397
47.67233	-103.641	701.7	1.85	397
47.67233	-103.641	701	1.84	397
47.67233	-103.641	700.7	1.85	397
47.67234	-103.641	700.4	1.84	397
47.67236	-103.641	700.7	1.84	397
47.67237	-103.641	700.9	1.85	397
47.67237	-103.641	701.2	1.83	397
47.67237	-103.641	701	1.84	397
47.67236	-103.64	701.1	1.83	397
47.67236	-103.64	700.9	1.84	397
47.67237	-103.64	700.6	1.85	397
47.67238	-103.64	700.9	1.85	397
47.67238	-103.64	701.4	1.85	397
47.67236	-103.64	701.4	1.85	397
47.67237	-103.64	701	1.85	397
47.67241	-103.64	700.6	1.85	397
47.67243	-103.64	700.5	1.84	397
47.67247	-103.64	701	1.85	397
47.67248	-103.64	701.5	1.84	397
47.67247	-103.64	702.1	1.85	397
47.67246	-103.64	701.5	1.85	398
47.67246	-103.64	700	1.83	398
47.67246	-103.64	699.8	1.83	398
47.67246	-103.64	699.4	1.84	398
47.67247	-103.64	698.9	1.83	398
47.67245	-103.641	699	1.84	398
47.67242	-103.641	699	1.83	398
47.67242	-103.641	699.6	1.83	398

47.67241	-103.641	700.3	1.84	398
47.67242	-103.641	700.3	1.84	398
47.67242	-103.641	700.3	1.84	398
47.67242	-103.641	700.3	1.84	398
47.67242	-103.641	700.3	1.84	398
47.67242	-103.641	700.6	1.84	398
47.67242	-103.641	700	1.84	398
47.67241	-103.641	699.1	1.84	398
47.67241	-103.641	698.8	1.83	398
47.67241	-103.641	699.5	1.84	398
47.67241	-103.641	701	1.84	398
47.67239	-103.641	701.5	1.84	398
47.67239	-103.641	701.8	1.84	397
47.67239	-103.641	702.2	1.83	397
47.6724	-103.641	702.8	1.83	397
47.6724	-103.641	702.9	1.84	397
47.67241	-103.641	702.8	1.84	397
47.67243	-103.641	703.1	1.84	397
47.67244	-103.641	703.6	1.84	397
47.67247	-103.641	702.4	1.83	397
47.6725	-103.641	702.5	1.84	397
47.6725	-103.641	702.6	1.84	397
47.6725	-103.641	702.1	1.83	397
47.67249	-103.641	702.9	1.84	397
47.67249	-103.641	702.8	1.84	397
47.67249	-103.641	702.6	1.85	397
47.67249	-103.641	702.4	1.83	397
47.67251	-103.641	701.9	1.83	397
47.67254	-103.641	702	1.84	397
47.67255	-103.641	702.8	1.85	397
47.67259	-103.641	703.3	1.84	397
47.6726	-103.641	703.4	1.84	397
47.6726	-103.641	704.2	1.84	397
47.6726	-103.641	705.2	1.85	397
47.6726	-103.641	705.7	1.83	397
47.6726	-103.641	705.9	1.84	397
47.67261	-103.641	706.7	1.84	397
47.67261	-103.641	707	1.83	397
47.6726	-103.641	706.8	1.84	397
47.67261	-103.641	706.3	1.84	397
47.67262	-103.641	706.3	1.83	397

47.67265	-103.641	706.3	1.84	397
47.67266	-103.641	705.6	1.84	397
47.67267	-103.641	705.4	1.84	397
47.67268	-103.641	705.3	1.84	397
47.67268	-103.641	704.7	1.84	397
47.67267	-103.641	705.6	1.84	397
47.67267	-103.641	705.8	1.83	397
47.67268	-103.641	706.3	1.84	397
47.67267	-103.641	705.9	1.84	397
47.67267	-103.641	706	1.84	397
47.67267	-103.641	705.6	1.84	397
47.67267	-103.64	704.8	1.84	397
47.67267	-103.64	705.6	1.84	397
47.67267	-103.64	705.7	1.84	397
47.67266	-103.64	706.7	1.83	397
47.67265	-103.64	706.4	1.84	397
47.67266	-103.64	705.4	1.83	397
47.6727	-103.64	704.6	1.83	397
47.67271	-103.64	704.4	1.84	397
47.67272	-103.64	703.5	1.84	397
47.67271	-103.64	703.1	1.83	397
47.67269	-103.64	703	1.84	397
47.67267	-103.64	702.5	1.84	397
47.67267	-103.64	701.9	1.84	397
47.67267	-103.64	701.7	1.84	397
47.67267	-103.64	701.6	1.83	397
47.67267	-103.64	701.4	1.83	397
47.67267	-103.64	700.9	1.83	397
47.67267	-103.64	700.2	1.84	397
47.67267	-103.64	700.5	1.83	397
47.67267	-103.641	700.5	1.83	397
47.67267	-103.641	700.9	1.83	397
47.67267	-103.641	700.9	1.83	397
47.67267	-103.641	701.1	1.84	397
47.67266	-103.641	701.2	1.84	397
47.67267	-103.641	702	1.83	397
47.67269	-103.641	702.9	1.84	397
47.6727	-103.641	702.8	1.84	397
47.67271	-103.641	702.3	1.83	397
47.67274	-103.641	701.9	1.83	397
47.67273	-103.641	701.5	1.83	397

47.67272	-103.641	701.5	1.83	397
47.67272	-103.641	701.1	1.83	397
47.67273	-103.641	701	1.83	397
47.67275	-103.641	701	1.84	397
47.67274	-103.641	700.6	1.84	397
47.67273	-103.641	700.3	1.83	397
47.67272	-103.641	699.9	1.84	397
47.67272	-103.64	699.2	1.83	397
47.67273	-103.64	699.2	1.83	397
47.67274	-103.64	699.5	1.83	397
47.67275	-103.64	699.9	1.84	397
47.67275	-103.64	699.9	1.84	397
47.67275	-103.64	699.9	1.83	397

Table IV: Field test data at well #2 – Trial #1

latitude	longitude	elevation	Methane conc. (ppm)	CO_2 conc. (ppm)
47.673302	-103.65846	721	1.87	399
47.673298	-103.65845	721	1.87	399
47.673306	-103.65845	721.1	1.87	399
47.673306	-103.65845	720.8	1.88	399
47.673309	-103.65844	720.5	1.87	399
47.673313	-103.65845	721.3	1.87	399
47.673275	-103.65845	722.4	1.86	398
47.673267	-103.65845	722.8	1.88	398
47.673271	-103.65845	723.2	1.86	398
47.673267	-103.65847	723.5	1.87	398
47.67326	-103.65852	723.7	1.87	398
47.673286	-103.65858	724.3	1.87	398
47.673351	-103.65863	724.5	1.86	398
47.673428	-103.65865	723.6	1.85	398
47.673492	-103.6586	723	1.87	398
47.673546	-103.65855	722.7	1.86	398
47.673603	-103.65852	722.7	1.87	399
47.673664	-103.65851	722.7	1.87	399
47.673721	-103.65849	722.7	1.87	399
47.673744	-103.65842	721.8	1.87	399
47.67374	-103.65829	721.8	1.86	399
47.673721	-103.65815	721.5	1.86	399
47.673729	-103.658	721.3	1.85	399
47.673737	-103.65782	721.5	1.87	399
47.673756	-103.65762	721.4	1.86	398
47.673775	-103.65742	721.7	1.87	398
47.673782	-103.65721	721.9	1.87	398
47.673771	-103.65699	723.2	1.86	398
47.673771	-103.65677	725.9	1.87	398
47.673779	-103.65656	727.9	1.86	398
47.673763	-103.65643	729	1.86	398
47.673744	-103.65631	730	1.86	398
47.673737	-103.65619	734.7	1.86	398
47.673763	-103.65611	735.4	1.85	398
47.673794	-103.65599	737.2	1.84	398
47.67382	-103.65585	739.2	1.85	398
47.67387	-103.65567	741.9	1.85	398
47.673927	-103.65549	743.3	1.87	398

47.673935	-103.65535	745.5	1.86	398
47.673866	-103.65527	746.5	1.86	398
47.673744	-103.65518	748.1	1.87	398
47.673637	-103.65509	749.9	1.86	398
47.673607	-103.65503	749.9	1.86	398
47.67363	-103.65507	749.3	1.87	398
47.673687	-103.65517	749.2	1.87	398
47.673683	-103.65549	748.6	1.85	398
47.673634	-103.65568	748.3	1.84	398
47.673573	-103.65588	748.9	1.85	398
47.673515	-103.65611	749.5	1.86	398
47.673462	-103.65636	748.9	1.86	398
47.673492	-103.65657	748.8	1.84	398
47.673603	-103.65673	749.5	1.86	398
47.673679	-103.65696	749.8	1.85	398
47.67371	-103.65722	749.7	1.86	398
47.673702	-103.6575	749.3	1.85	398
47.67366	-103.65779	749	1.85	398
47.673603	-103.65808	750	1.84	398
47.673565	-103.65834	750.5	1.85	398
47.673542	-103.65855	750.1	1.85	398
47.673542	-103.65855	750.8	1.85	398
47.673542	-103.65852	751.8	1.85	398
47.673542	-103.6585	752	1.85	398
47.673542	-103.65849	752.8	1.85	398
47.673542	-103.65849	753	1.86	398
47.673531	-103.65849	753	1.86	398
47.673492	-103.65845	752.9	1.85	398
47.673454	-103.65836	753.2	1.85	398
47.673439	-103.65833	753	1.85	398
47.673435	-103.65828	752.7	1.84	398
47.673447	-103.65813	752.7	1.84	398
47.673481	-103.65793	752.9	1.85	398
47.673523	-103.65769	753.2	1.85	398
47.673557	-103.65742	753.2	1.84	398
47.673561	-103.65712	752.4	1.85	398
47.673542	-103.6568	752.3	1.84	398
47.673519	-103.65647	752.4	1.84	398
47.673622	-103.65565	753	1.84	398
47.673737	-103.65541	753.7	1.83	398
47.67379	-103.65525	753.5	1.84	398

47.673786	-103.65524	754.2	1.83	398
47.673748	-103.6552	754.6	1.85	398
47.673679	-103.65512	754.4	1.84	398
47.673607	-103.65505	753	1.84	398
47.673534	-103.65503	750.9	1.84	398
47.673477	-103.65508	745.8	1.84	398
47.673447	-103.65511	744.8	1.85	398
47.673443	-103.65511	744.7	1.85	398
47.673435	-103.65517	744.4	1.84	398
47.67342	-103.65531	743.5	1.84	398
47.673397	-103.6555	742.1	1.83	398
47.673389	-103.65573	740.9	1.84	397
47.673378	-103.65624	738.8	1.83	397
47.673359	-103.65651	738.3	1.83	397
47.67334	-103.65678	738.4	1.83	397
47.673328	-103.65703	738	1.83	397
47.673317	-103.65727	737.8	1.84	397
47.673302	-103.65752	737.6	1.84	397
47.67329	-103.65776	737.4	1.83	397
47.673279	-103.65801	737	1.83	397
47.67326	-103.65825	735.9	1.83	397
47.673248	-103.65849	735.9	1.83	397
47.673233	-103.65857	735.2	1.84	397
47.673222	-103.65857	734.1	1.83	397
47.67318	-103.65858	733.9	1.84	397
47.673107	-103.65857	734	1.84	397
47.673038	-103.65854	733.1	1.84	397
47.673	-103.65845	732.6	1.84	397
47.672997	-103.65836	731.6	1.83	397
47.673016	-103.65823	729.7	1.83	397
47.673054	-103.65809	729.2	1.84	397
47.6731	-103.65792	729.5	1.84	397
47.67313	-103.65775	730.6	1.83	397
47.673153	-103.65759	731	1.83	397
47.673161	-103.65744	731.5	1.84	397
47.673164	-103.65732	731.2	1.83	397
47.673157	-103.6572	732.2	1.83	397
47.673157	-103.65709	732.4	1.83	397
47.673157	-103.65694	733	1.83	397
47.673157	-103.65675	733.5	1.84	397
47.673153	-103.6565	734.3	1.84	398

47.673149	-103.65623	734.9	1.83	398
47.673149	-103.65595	735.4	1.84	397
47.673149	-103.65568	735.6	1.84	397
47.673153	-103.65543	736.7	1.83	397
47.673153	-103.65521	736.9	1.84	397
47.673145	-103.65515	736.4	1.84	397
47.673141	-103.65513	734.7	1.84	397
47.673107	-103.65511	735.3	1.83	397
47.673031	-103.65511	735.1	1.84	397
47.672962	-103.65511	733.8	1.83	397
47.672901	-103.65514	733.9	1.84	397
47.672894	-103.65524	735.2	1.83	397
47.67289	-103.6554	735.3	1.83	397
47.672897	-103.6556	734.4	1.83	397
47.672913	-103.65583	733.4	1.83	397
47.672897	-103.65636	733.4	1.82	397
47.672867	-103.65663	733.3	1.82	397
47.672852	-103.6569	732.7	1.83	397
47.672867	-103.65716	732.5	1.83	397
47.672905	-103.65742	732.3	1.83	397
47.672928	-103.65768	732	1.84	397
47.672932	-103.65795	731.9	1.84	397
47.672916	-103.65821	731.9	1.83	397
47.672894	-103.65834	731.9	1.84	397
47.672882	-103.65845	731.8	1.83	397
47.672848	-103.65853	731.4	1.84	397
47.672752	-103.65854	730.9	1.83	397
47.672676	-103.65848	730.7	1.84	397
47.672626	-103.65832	731.2	1.83	397
47.672615	-103.65811	732.1	1.84	397
47.672646	-103.65789	732.5	1.84	397
47.672691	-103.65767	732.8	1.83	397
47.672707	-103.65741	732.9	1.83	397
47.672691	-103.65713	732.5	1.84	397
47.672665	-103.65683	732.6	1.83	397
47.672646	-103.65654	732.9	1.84	397
47.672642	-103.65624	733	1.83	397
47.672646	-103.65595	732.6	1.83	397
47.672672	-103.65566	732.9	1.84	397
47.672714	-103.65537	733	1.83	397
47.672729	-103.65518	732.6	1.83	397

47.672718	-103.65515	732	1.84	397
47.67268	-103.65511	731.6	1.83	397
47.672611	-103.65508	732.3	1.84	397
47.672543	-103.6551	733.4	1.83	397
47.672501	-103.65517	733.9	1.84	397
47.672493	-103.65531	733.7	1.83	397
47.672527	-103.6555	733.4	1.84	397
47.672585	-103.65573	733.2	1.84	397
47.672611	-103.65587	733.1	1.83	397
47.672611	-103.65595	733	1.83	397
47.672588	-103.65612	732.8	1.83	397
47.67252	-103.65631	732.5	1.83	398
47.672443	-103.65648	730.7	1.83	398
47.672398	-103.65668	723.5	1.83	398
47.672398	-103.65689	718.1	1.83	398
47.672398	-103.65694	715.6	1.83	398
47.672401	-103.65694	716.8	1.83	398
47.672401	-103.65694	716.3	1.83	398
47.672401	-103.65692	716.7	1.84	398
47.672401	-103.65692	716.7	1.84	398
47.672401	-103.65692	716.4	1.84	398
47.672401	-103.65691	716.1	1.84	398
47.672401	-103.65691	716	1.84	398
47.672401	-103.65691	715.8	1.83	398
47.672401	-103.65691	715.6	1.84	398
47.672401	-103.65691	715.3	1.84	398
47.672401	-103.65691	715.1	1.84	398
47.672401	-103.65691	715.2	1.84	398
47.672401	-103.65691	715.4	1.84	398
47.672401	-103.6569	715.4	1.84	398
47.672401	-103.6569	715.4	1.84	398
47.672401	-103.6569	715.2	1.84	398
47.672401	-103.6569	715.2	1.84	398
47.672398	-103.6569	715.3	1.83	398
47.672398	-103.6569	715.2	1.83	398
47.672398	-103.6569	715.1	1.83	398
47.672398	-103.6569	715	1.83	398
47.672398	-103.6569	715	1.83	398
47.672398	-103.6569	714.9	1.84	398
47.672398	-103.6569	714.9	1.83	398
47.672398	-103.6569	714.9	1.83	398

47.672398	-103.6569	714.9	1.84	398
47.672398	-103.6569	714.9	1.84	398
47.672398	-103.6569	715	1.83	398
47.672398	-103.6569	715	1.84	398
47.672398	-103.6569	715	1.83	398
47.672398	-103.6569	715	1.84	398
47.672398	-103.6569	714.9	1.84	398
47.672398	-103.6569	715.1	1.84	398
47.672394	-103.65689	715.1	1.84	398
47.672394	-103.65689	715	1.84	398
47.672394	-103.65689	715	1.84	398
47.672394	-103.65689	715.2	1.84	398
47.672394	-103.65689	715.3	1.84	398
47.672394	-103.65689	715.3	1.84	398
47.672394	-103.65689	715.2	1.83	398
47.672394	-103.65689	715.1	1.84	398
47.672394	-103.65689	714.9	1.83	398
47.672394	-103.65689	714.8	1.84	398
47.672394	-103.65689	714.7	1.83	398
47.672386	-103.65689	714.5	1.83	398
47.672394	-103.65689	714.4	1.83	398
47.672394	-103.65689	714.5	1.83	398
47.672394	-103.65689	714.5	1.83	398
47.672398	-103.65689	714.5	1.84	398
47.672398	-103.65689	714.5	1.83	398
47.672398	-103.65688	714.5	1.83	398
47.672401	-103.65688	714.5	1.83	398
47.672398	-103.65688	714.8	1.84	398
47.672409	-103.65688	715.4	1.83	398
47.672432	-103.65689	715.4	1.84	398
47.672459	-103.6569	715.2	1.83	398
47.672485	-103.65691	715	1.83	398
47.672508	-103.65693	715	1.83	398
47.672535	-103.65694	714.8	1.83	398
47.672554	-103.65697	715.3	1.83	398
47.672573	-103.65701	715.5	1.83	398
47.672588	-103.65703	715.2	1.83	398
47.672604	-103.65704	713.9	1.84	398
47.672626	-103.65704	713	1.83	398
47.672653	-103.65706	712.4	1.84	398
47.672684	-103.65707	712.5	1.83	398

47.672722	-103.65709	712.8	1.84	398
47.672741	-103.6571	713	1.84	398
47.672756	-103.65714	712	1.84	398
47.672764	-103.65717	712	1.84	398
47.672768	-103.6572	712.5	1.83	398
47.67276	-103.65723	711.5	1.83	398
47.67276	-103.65726	711.7	1.83	398
47.67276	-103.6573	711.4	1.84	398
47.672771	-103.65735	711.8	1.83	398
47.672775	-103.65739	711.5	1.83	398
47.672775	-103.65742	711.7	1.83	397
47.672775	-103.65746	711.8	1.83	397
47.672783	-103.6575	712.1	1.83	397
47.672787	-103.65755	712.2	1.83	397
47.672791	-103.65759	712.2	1.83	397
47.672798	-103.65762	711.9	1.83	397
47.672806	-103.65766	711.6	1.84	397
47.672813	-103.6577	711.6	1.83	397
47.672825	-103.65774	711.5	1.84	397
47.672825	-103.65778	711.4	1.83	397
47.672825	-103.65783	711.3	1.83	397
47.672825	-103.65787	711.5	1.84	397
47.672829	-103.65791	711.9	1.83	397
47.672836	-103.65796	711.4	1.84	397
47.67284	-103.658	711.3	1.84	397
47.672844	-103.65805	711.6	1.85	397
47.672855	-103.65809	711.4	1.84	397
47.672882	-103.65811	711.6	1.84	397
47.672909	-103.65813	711.7	1.84	397
47.672935	-103.65815	711.8	1.84	397
47.672958	-103.65818	711.8	1.84	397
47.672985	-103.6582	711.5	1.85	397
47.673012	-103.65822	711.5	1.85	397
47.673035	-103.65824	711.5	1.84	397
47.673061	-103.65826	711.5	1.84	397
47.673084	-103.65829	711.8	1.84	397
47.673111	-103.65832	711.5	1.84	397
47.673138	-103.65833	711.2	1.84	397
47.673164	-103.65836	711.1	1.84	397
47.673191	-103.65839	711.1	1.83	397
47.67321	-103.65842	711.1	1.84	397

47.673229	-103.65845	711.3	1.83	397
47.673248	-103.65849	711.3	1.83	396
47.673271	-103.6585	711.5	1.83	396
47.673271	-103.65849	711.7	1.84	396
47.673275	-103.65849	711.5	1.83	396
47.673271	-103.65849	711.4	1.83	396
47.673275	-103.65849	711.5	1.83	396
47.673275	-103.65849	711.6	1.83	396
47.673271	-103.65849	711.9	1.83	396
47.673271	-103.65849	712.4	1.83	396
47.673271	-103.65849	712.4	1.84	396
47.673271	-103.65849	712.3	1.83	396
47.673275	-103.65849	712.4	1.84	396
47.673275	-103.65849	712.8	1.83	396
47.673279	-103.65849	712.8	1.83	396
47.673279	-103.65849	712.9	1.83	396
47.673279	-103.6585	712.5	1.83	396
47.673283	-103.6585	712.8	1.83	396
47.673286	-103.65851	712.7	1.84	396
47.673286	-103.65851	712.8	1.83	396
47.673283	-103.65851	712.3	1.83	396
47.673283	-103.65851	712	1.84	396
47.673286	-103.65851	711.9	1.84	396
47.673286	-103.65851	712.1	1.84	396
47.67329	-103.65851	712.7	1.83	396
47.67329	-103.65852	713.2	1.83	396
47.67329	-103.65852	713.7	1.83	396
47.67329	-103.65852	713.4	1.83	396
47.67329	-103.65852	713.4	1.83	396
47.67329	-103.65852	713.6	1.83	396
47.67329	-103.65852	713.7	1.83	396
47.67329	-103.65852	714	1.83	396
47.67329	-103.65853	713.9	1.84	396
47.67329	-103.65853	713.8	1.83	396
47.67329	-103.65853	714	1.83	396
47.67329	-103.65853	713.7	1.83	396
47.673286	-103.65853	713.3	1.84	396
47.673286	-103.65854	713.2	1.83	396
47.673286	-103.65854	713.5	1.84	396
47.673286	-103.65854	713.4	1.84	396
47.673286	-103.65854	713.7	1.84	396

47.673286	-103.65854	713.6	1.84	396
47.673286	-103.65854	713.6	1.83	396
47.673286	-103.65854	713.5	1.83	396
47.673286	-103.65854	713.7	1.83	396
47.673283	-103.65854	714	1.83	396
47.673283	-103.65854	713.8	1.84	396
47.673283	-103.65854	713.7	1.83	396
47.673279	-103.65854	713.4	1.84	396
47.673279	-103.65854	713.2	1.84	396
47.673279	-103.65854	713.4	1.83	396
47.673279	-103.65854	713.4	1.84	396
47.673279	-103.65854	713.5	1.83	396
47.673279	-103.65854	713.4	1.83	396
47.673279	-103.65854	713.4	1.83	396
47.673279	-103.65854	713.3	1.83	396
47.673275	-103.65854	713.3	1.84	396
47.673275	-103.65854	713.1	1.84	396
47.673275	-103.65854	713.3	1.83	396
47.673275	-103.65854	713.8	1.83	396
47.673279	-103.65854	714.3	1.84	396
47.673283	-103.65854	714.3	1.84	396
47.673286	-103.65854	713.8	1.83	396
47.673286	-103.65854	713.7	1.84	396
47.673286	-103.65854	713.7	1.83	396
47.673286	-103.65854	713.7	1.83	396
47.673283	-103.65854	713.4	1.83	396
47.673286	-103.65854	713.3	1.83	396
47.673286	-103.65854	713.3	1.83	396
47.673286	-103.65854	713.4	1.83	396
47.673286	-103.65854	713.7	1.84	396
47.673286	-103.65854	713.3	1.83	396
47.673286	-103.65854	712.6	1.83	396
47.67329	-103.65854	712.6	1.83	396
47.67329	-103.65854	712	1.84	396
47.673286	-103.65853	712.6	1.84	396
47.673286	-103.65853	712.9	1.83	396
47.673283	-103.65853	713.3	1.83	396
47.673283	-103.65853	713.3	1.83	396
47.673279	-103.65853	713.7	1.83	396
47.673279	-103.65852	713.6	1.83	396
47.673275	-103.65852	713.6	1.84	396

47.673279	-103.65852	713.7	1.83	396
47.673279	-103.65852	713.7	1.84	396
47.673283	-103.65852	713.8	1.83	396
47.673283	-103.65852	713.5	1.84	396
47.673283	-103.65851	713.1	1.84	396
47.673279	-103.6585	712.8	1.83	396
47.673279	-103.6585	712.8	1.83	396
47.673279	-103.65849	712.6	1.83	396
47.673275	-103.65849	712.5	1.83	396
47.673275	-103.65849	712.1	1.83	396
47.673275	-103.65848	711.9	1.83	396
47.673275	-103.65848	712.1	1.84	396
47.673275	-103.65847	712.2	1.83	396
47.673275	-103.65847	712.6	1.83	396
47.673275	-103.65847	712.8	1.84	396
47.673271	-103.65847	712.9	1.83	396
47.673271	-103.65847	713	1.84	396
47.673271	-103.65848	713.1	1.83	396
47.673271	-103.65847	713.2	1.83	396
47.673271	-103.65847	713.1	1.83	396
47.673267	-103.65847	713	1.83	396
47.673267	-103.65847	713.1	1.83	396
47.673271	-103.65847	712.9	1.83	396
47.673267	-103.65847	712.8	1.84	396
47.673267	-103.65847	712.4	1.83	396
47.673264	-103.65847	711.8	1.84	396
47.673264	-103.65847	711.5	1.83	396
47.673264	-103.65847	711.5	1.83	396
47.67326	-103.65846	711.5	1.83	396
47.673256	-103.65846	711.6	1.83	396
47.67326	-103.65846	711.7	1.83	396
47.67326	-103.65845	712.2	1.83	396
47.673264	-103.65845	712.4	1.84	396
47.673264	-103.65845	712.9	1.84	396
47.673264	-103.65845	713.2	1.84	396
47.673264	-103.65845	713.4	1.83	396
47.673267	-103.65845	713.3	1.83	396
47.673264	-103.65845	713.2	1.83	396
47.673264	-103.65846	713.1	1.83	396
47.673267	-103.65845	713.4	1.83	396
47.673267	-103.65845	713.3	1.83	396

47.673264	-103.65845	713.4	1.84	396
47.673256	-103.65845	713.9	1.83	396
47.673256	-103.65845	713.8	1.84	396
47.67326	-103.65845	713.5	1.84	396
47.67326	-103.65845	713.4	1.83	396
47.67326	-103.65845	713.9	1.84	396
47.67326	-103.65845	714.3	1.82	396
47.673264	-103.65845	714	1.83	396
47.67326	-103.65846	714.1	1.83	396
47.673264	-103.65846	714.3	1.83	396
47.673264	-103.65846	714.4	1.83	396
47.673264	-103.65846	714.3	1.84	396
47.673267	-103.65846	714.4	1.83	396
47.673271	-103.65847	714.3	1.84	396
47.673275	-103.65847	714.6	1.83	396
47.673275	-103.65847	714.6	1.83	396
47.673275	-103.65847	714.9	1.83	396
47.673275	-103.65847	715	1.83	396
47.673275	-103.65847	714.9	1.83	396
47.673271	-103.65846	714.1	1.83	396
47.673271	-103.65846	712.8	1.83	396
47.673275	-103.65847	712.6	1.83	396
47.673275	-103.65847	712.4	1.83	396
47.673271	-103.65847	712.2	1.83	396
47.673271	-103.65847	712.2	1.83	396
47.673271	-103.65847	712.2	1.82	396
47.673267	-103.65847	712.2	1.83	396
47.673267	-103.65847	711.7	1.83	396
47.673267	-103.65847	711.7	1.83	396
47.673264	-103.65847	711.5	1.83	396
47.673264	-103.65847	711.5	1.83	396
47.673264	-103.65847	711.6	1.84	396
47.673267	-103.65847	711.7	1.83	396
47.673267	-103.65847	711.6	1.83	396
47.673267	-103.65847	711.6	1.83	396
47.673271	-103.65847	711.6	1.83	396
47.673271	-103.65847	711.7	1.84	396
47.673271	-103.65847	711.7	1.83	396
47.673271	-103.65847	711.8	1.83	396
47.673271	-103.65847	711.8	1.84	396
47.673275	-103.65847	711.9	1.83	396

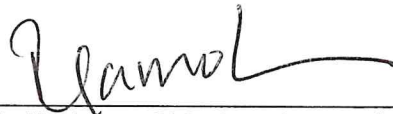|				
47.673275	-103.65847	711.9	1.83	396
47.673275	-103.65847	712	1.82	396
47.673275	-103.65847	711.9	1.83	396
47.673275	-103.65847	711.7	1.83	396
47.673275	-103.65848	711.7	1.83	396
47.673275	-103.65848	711.9	1.83	396

SIGNATURE PAGE

This is to certify that the thesis prepared by Siwen Liu entitled "Development of a UAV-Based System to Monitor Air Quality over an Oil Field" has been examined and approved for acceptance by the Department of Environmental Engineering, Montana Technological University, on this 30th day of November, 2018.

Xufei Yang, PhD, Assistant Professor
Department of Environmental Engineering
Chair, Examination Committee

Raja Nagisette, PhD, Associate Professor
Department of Environmental Engineering
Member, Examination Committee

Xiaobing Zhou, PhD, Professor
Department of Geophysical Engineering
Member, Examination Committee